Topology Design with Optimized, Self-Adaptive Materials

C. S. JOG and R. B. HABER
Department of Theoretical and Applied Mechanics
University of Illinois at Urbana-Champaign
Urbana, Illinois
U.S.A

M. P. BENDSØE
Matematisk Institut
Danmarks Tekniske Højskole
Lyngby
Denmark

Abstract:

Significant performance improvements can be obtained if the topology of an elastic structure is allowed to vary in shape optimization problems. We study the optimal shape design of a two-dimensional elastic continuum for minimum compliance subject to a constraint on the total volume of material. The macroscopic version of this problem is not well-posed if no restrictions are placed on the structure topology; relaxation of the optimization problem via quasiconvexification or homogenization methods is required. The effect of relaxation is to introduce a perforated microstructure that must be optimized simultaneously with the macroscopic distribution of material.

A combined analytical-computational approach is proposed to solve the relaxed optimization problem. Both stress and displacement analysis methods are presented. Since rank-2 layered composites are known to achieve optimal energy bounds, we restrict the design space to this class of microstructures whose effective properties can easily be determined in explicit form. We develop a series of reduced problems by sequentially interchanging extremization operators and analytically optimizing the microstructural design fields. This results in optimization problems involving the distribution of an adaptive material that continuously optimizes its microstructure in response to the current state of stress or strain. A further reduced problem, involving only the response field, can be obtained in the stress-based approach, but the requisite interchange of extremization operators is not valid in the case of the displacement-based model.

Finite element optimization procedures based on the reduced displacement formulation are developed and numerical solutions are presented. Care must be taken in selecting the discrete function spaces for the design density and displacement response, since the reduced problem is a two-field, mixed variational problem. An improper choice for the solution space leads to instabilities in the optimal design similar to those encountered in mixed formulations of the Stokes problem.

1 Introduction

The problem of shape optimization is of great interest to the structural optimization community. Shape optimization involves redistributing material to optimize the objective function. Three classes of shape optimization problems are worthy of mention. *Sizing* shape optimization problems allow for changes in section properties (area, moment of inertia, thickness, etc.), with the underlying manifold that defines the geometry of the structure fixed[1]. *Fixed topology* shape optimization problems allow for changes in the manifold configuration, but not its connectivity. For example, one could change the joint positions in a truss or vary the boundary of a continuum structure. This class of problems has received considerable attention recently, and there are well-established tools for describing shape changes under a fixed topology. The literature on this class of methods has been surveyed by Ding [1], Haftka and Gandhi [2] and Haber *et. al.* [3]. *Variable topology* shape optimization problems allow for arbitrary changes in the manifold geometry, including connectivity. For example, one could change the number or connectivity of the joints in a truss or introduce multiply-connected regions in a continuum structure. In general, it is possible to achieve significant improvements in performance if the topology of the structure is allowed to vary in shape optimization problems. For example, suppose the optimal geometry for a given structural design problem contains a circular hole, but the initial design topology is simply connected. Then a fixed-topology optimization method cannot generate the optimal design.

The earliest literature on topology optimization problems involves layout problems. For example, Prager, Rozvany and others have studied the problem of layout optimization for structures with many thin, 'truss-like' members ([4], [5]). A direct approach to continuum optimization over variable topologies would involve a search for the optimal macroscopic partition of the candidate structural domain into solid and void regions, as for example described in [6]. However, it was found in several studies on the problem of design with two dissimilar materials ([7]-[11])that this formulation of the topology problem

1. Most authors would not classify these as shape optimization problems, but we mention them here because they do involve variations in the three-dimensional geometry of the structure.

is not well-posed. The reasons for the ill-posedness are similar to those that complicate the optimization of variable-thickness Kirchoff plates [12]. Kohn and Strang obtained a well-posed, relaxed formulation for 2-D conductivity by quasiconvexification and, alternatively, by introducing microstructure to the material model [7]. The main advantage of this relaxed formulation is that the resulting optimization problem is well-posed and, in the case of finite element models, the solution is no longer mesh-dependent. The disadvantage is that the optimal design might include regions with a perforated microstructure that is generally impractical for manufacture. The relaxed problem can be approximated using a fixed or adaptively-varying finite element grid on a fixed domain, with the bulk density of the composite to be determined at each point of the domain [13]. Bendsøe and Kikuchi explored this approach using simple microstructures that approximate the optimal microstructural configuration [14].

In this study we are concerned with topology optimization procedures based on an exact optimal microstructure. Studies on the bounds of the effective material properties of composite mixtures show that the stiffest material for a structure under conditions of plane stress can be obtained using a rank-2 composite ([15]-[21]). A rank-2 composite is characterized by the orientation of its layers with respect to the global coordinate axes and by the densities of its layers (see Section 3). If the orientation and layer densities of a rank-2 composite are known, then the effective material properties can be found using the formulas of homogenization [22]. Note that rank-2 materials are not the only family of composites which can achieve the upper bound on the stiffness of a mixture of two materials ([23], [24]). However, they are a convenient choice for our purposes since the effective material properties can be expressed as fairly simple, explicit rational functions of the layer densities. This is crucial for the development that follows.

In the following sections, we develop displacement and stress-based formulations of the relaxed topology optimization problem and carry out analytical optimization of the distributed microstructural design parameters. We obtain a reduced problem in the form of a two-field, inf-sup problem that generates a mixed finite element method.

2 Statement of the Topology Optimization Problem

We consider the problem of finding the stiffest structure that can be obtained by distributing a given volume of material $\bar{V}$ within a domain $\Omega \subset R^2$. We assume a homogeneous, linear elastic, isotropic material, small deformations, plane stress conditions, a single static loading case and that all interior boundaries are traction free.

We present the strong forms of the governing equations and the boundary conditions and the corresponding variational problems. The section closes with the formulation of the topology optimization problem.

2.1 STRONG FORM OF THE BOUNDARY VALUE PROBLEM

Let Ω be an open domain with boundary Γ. The boundary is composed of two open, disjoint regions, $\Gamma = \overline{\Gamma_u \cup \Gamma_t}$. The following governing equations and boundary conditions apply.

$$\nabla \cdot \sigma + \boldsymbol{b} = 0 \text{ in } \Omega \tag{1}$$

$$\varepsilon(\boldsymbol{u}) = \frac{1}{2}(\nabla \boldsymbol{u} + (\nabla \boldsymbol{u})^T) \text{ in } \Omega \tag{2}$$

$$\sigma = \boldsymbol{C}:\varepsilon \text{ in } \Omega \tag{3}$$

$$\boldsymbol{t} = \sigma \cdot \boldsymbol{n} \text{ on } \Gamma \tag{4}$$

$$\boldsymbol{u} = \bar{\boldsymbol{u}} \text{ on } \Gamma_u \tag{5}$$

$$\boldsymbol{t} = \bar{\boldsymbol{t}} \text{ on } \Gamma_t \tag{6}$$

σ is the stress tensor, $\boldsymbol{u}$ is the displacement vector, ε is the strain tensor, $\boldsymbol{b}$ is the body force vector, $\boldsymbol{t}$ is the traction vector, $\boldsymbol{n}$ is the unit normal vector to the surface Γ, $\bar{\boldsymbol{u}}$ is a vector of prescribed displacements, $\bar{\boldsymbol{t}}$ is a vector of prescribed tractions and $\boldsymbol{C}$ is the material stiffness tensor.

2.2 VARIATIONAL FORMS OF THE GOVERNING EQUATIONS

We first replace the strong form of the problem with a weak form using the principle of minimum potential energy:

Find the displacement field u^* that solves $\min_{u \in V_u} \Pi(u)$ such that equations (2)-(4) are satisfied, where

$$\Pi(u) = \int_{\Omega} W(\varepsilon(u))\, d\Omega - \int_{\Gamma_t} (\bar{t} \cdot u)\, d\Gamma - \int_{\Omega} (b \cdot u)\, d\Omega \tag{7}$$

and $V_u = \{u \in H^1(\Omega) \ : \ u = \bar{u} \text{ on } \Gamma_u\}$.

W is the strain energy density function which, for a linear elastic material, is given by,

$$W(\varepsilon) = \frac{1}{2}\varepsilon^T C \varepsilon \tag{8}$$

Alternatively, if we base the formulation on the principle of minimum complementary energy we obtain,

Find σ^* which solves $\min_{\sigma \in V_\sigma} \Pi_c(\sigma)$ such that equations (3) and (4) are satisfied,

where

$$\Pi_c(\sigma) = \int_{\Omega} W_c(\sigma)\, d\Omega - \int_{\Gamma_u} (t \cdot \bar{u})\, d\Gamma \tag{9}$$

and $V_\sigma = \{\sigma \in L_2(\Omega) \ : \ (\nabla \cdot \sigma) + b = 0 \text{ in } \Omega \ , \ (\sigma \cdot n) = \bar{t} \text{ on } \Gamma_t\}$.

W_c is the complementary energy density for a linear elastic material given by,

$$W_c(\sigma) = \frac{1}{2}\sigma^T D \sigma \ ; \qquad D = C^{-1} \tag{10}$$

2.3 THE TOPOLOGY OPTIMIZATION PROBLEM

We are interested in finding a configuration of solid and void regions within the domain Ω that maximizes the stiffness of the resulting structure, such that the total volume of material equals a specified value $\bar{V}$. No restriction is placed on the topology of the configuration of the solid part of Ω. One way to formulate this problem is to introduce the indicator function $X(x)$ given by,

$$X(x) = \begin{cases} 1 \text{ if } x \in \Omega_s \\ 0 \text{ if } x \in \Omega_v \end{cases} \tag{11}$$

where Ω_s and Ω_v are the solid and void regions in Ω, respectively, as shown in Fig. 1. The volume of the structure is given by $\int_{\Omega} X(x)\, d\Omega$ and the elasticity tensor at each point is $C = X(x)\, C_{solid}$ where C_{solid} is the elasticity tensor of the solid material.

The following *compliance functional* measures the flexibility of the structure.

$$J = \int_{\Gamma_t} (\bar{t} \cdot \boldsymbol{u})\, d\Gamma - \int_{\Gamma_u} (\boldsymbol{t} \cdot \bar{\boldsymbol{u}})\, d\Gamma + \int_{\Omega} (\boldsymbol{b} \cdot \boldsymbol{u})\, d\Omega \tag{12}$$

Maximizing the stiffness of a structure corresponds to minimizing the compliance J. For a linear elastic material, Clapeyron's work theorem [27] gives the following relations.

$$\Pi = -\frac{J}{2} \tag{13}$$

$$\Pi_c = \frac{J}{2} \tag{14}$$

Therefore, maximizing the stiffness is equivalent to minimizing the complementary energy or maximizing the potential energy. Alternative forms of the maximum stiffness problem are stated as:

- Displacement formulation:

$$\sup_{X(x) \in V_x} \quad \inf_{u \in V_u} \quad \int_\Omega W(\varepsilon(u))\, d\Omega - \int_{\Gamma_t} (\bar{t} \cdot u)\, d\Gamma - \int_\Omega (b \cdot u)\, d\Omega \tag{15}$$

where $C = X(x)\, C_{solid}$

- Stress formulation

$$\inf_{X(x) \in V_x} \cdot \inf_{\sigma \in V_\sigma} \quad \int_\Omega W_c(\sigma)\, d\Omega - \int_{\Gamma_u} ((\sigma \cdot n) \cdot \bar{u})\, d\Gamma \tag{16}$$

where $D = X(x)\, D_{solid}$.

The set of admissable designs for the above problems is defined as,

$$V_x = \{ Y : Y(x) = 0 \text{ or } 1 \quad \forall x \in \Omega, \int_\Omega Y(x)\, d\Omega = \bar{V} \}.$$

The above macroscopic design problem is not well-posed in the sense that the space of allowable designs is not closed under the introduction of fine-scale oscillations of the indicator function. This is a feature of all design problems of the general form described above, which involve a general variation of the coefficients of the high-order terms of an elliptic operator ([7]-[11]). As a result, attempts to optimize finite element models based on the macroscopic approach would fail to converge to a macroscopic pattern of solid and void regions in the limit of mesh refinement - a feature that was first seen in an analysis of the analogous variable thickness Kirchoff plate design problem, as studied by Cheng and Olhoff [12]. Kohn and Strang showed that a tractable, relaxed form of the two-dimensional, scalar conduction problem can be obtained either by quasiconvexification of the macroscopic optimization problem or, equivalently, by introducing microstructure to the design space ([7], [25]). The process of relaxation leads to a well-posed problem and tends to eliminate artificial local minima that arise in the macroscopic optimization problem [13]. In this paper, we work with both the displacement and stress-based elasticity formulations described above and perform relaxation via knowledge of optimal composites. In a recent parallel development, Allaire and Kohn extended the direct relaxation approach to the

stress-based elasticity problem [26]. The introduction of microstructure transforms the optimization task from the determination of the indicator function $X(x)$ to the determination of distributions of microstructural parameters, as explained below.

3 Optimum Material Distribution and Effective Material Properties

Studies of the bounds on the effective properties of composite mixtures of two materials show that for plane elasticity, the stiffest composite material for a fixed ratio of the two constituent materials can be obtained by a rank-2 layering, as shown in Fig. 2 ([15]-[19]; see [20], [21] for a comprehensive discussion). The rank-2 composite is constructed as follows. First, a rank-1 composite is constructed of alternating layers of the stiffer and the more flexible materials. The averaged densities of the stiff and flexible layers are designated γ and $1-\gamma$, respectively. The rank-2 composite is then constructed of alternating layers of the stiff material and the rank-1 composite with average densities δ and $1-\delta$, respectively. The characteristic length scales of the rank-1 and rank-2 layerings must be of different orders of magnitude ($L_1 \ll L_2$). Furthermore, the rank-1 layering direction is perpendicular to the rank-2 direction. The bulk density of the stiff material is,

$$\rho = \delta + \gamma - \gamma\delta \tag{17}$$

In the context of shape optimization of a homogeneous material with voids, we assign void properties ($X = 0$) to the flexible material in the rank-2 composite. Then ρ in equation (17) gives the bulk density of the rank-2 material and the volume constraint is expressed as,

$$\int_{\Omega} \rho \, d\Omega = \bar{V} \tag{18}$$

The effective material properties of the rank-2 composite can be derived using the formulas of homogenization [22]. Assuming that the primary layering of density δ is aligned along the direction 2 (as shown in Fig. 2), the effective properties for the rank-2 composite can be computed by iterative application of the formulas for a rank-1 layering [28] or by

invoking the general formula for a rank-N layering, as developed by Francfort and Murat [29]. Following the former approach, we obtain

$$C_{1111} = \frac{\gamma E}{\delta\gamma(1-\nu^2) + (1-\delta)} \qquad C_{2222} = \delta E + \delta^2\nu^2 C_{1111}$$
$$C_{1122} = \frac{\nu\delta\gamma E}{\delta\gamma(1-\nu^2) + (1-\delta)} \qquad C_{1212} = 0 \tag{19}$$

where E is the Young's modulus and ν is the Poisson's ratio of the solid isotropic material. The tensor components in (19) correspond to the effective properties of the homogenized material in a material coordinate system that is inclined at an angle θ to the global reference frame (Fig. 2). The effective properties in the global reference frame can be found using the standard coordinate transformation formulas for the elasticity tensor.

The process of relaxation expands the macroscopic design space, and the outer subproblems in (15) and (16) are transformed accordingly. Now we seek the supremum of the potential energy (or the infimum of the complementary potential energy) over $\theta(x)$, $\delta(x)$ and $\gamma(x)$ instead of $X(x)$. The analytical optimization of these functions is discussed in the following section.

4 Analytical Optimization Of the Microscopic Design Functions

We now express the displacement and stress formulations in terms of the variables θ, δ and γ in $L_\infty(\Omega)$.

- Displacement problem DP0:

$$\sup_{\theta,\delta,\gamma} \quad \inf_{u \in V_u} \quad L_u(\theta, \delta, \gamma, u) \tag{20a}$$

subject to $0 \le \delta \le 1$, $0 \le \gamma \le 1$, $\rho = \delta + \gamma - \gamma\delta$ and $\int_\Omega \rho d\Omega = \bar{V}$;

$$L_u(\theta, \delta, \gamma, u) = \int_\Omega W(\varepsilon(u))\, d\Omega - \int_{\Gamma_t} (\bar{t} \cdot u)\, d\Gamma - \int_\Omega (b \cdot u)\, d\Omega \tag{20b}$$

- Stress problem SP0:

$$\inf_{\theta,\delta,\gamma} \quad \inf_{\sigma \in V_\sigma} \quad L_\sigma(\theta, \delta, \gamma, \sigma) \tag{21a}$$

subject to $0 \le \delta \le 1$, $0 \le \gamma \le 1$, $\rho = \delta + \gamma - \gamma\delta$ and $\int_\Omega \rho d\Omega = \bar{V}$;

$$L_\sigma(\theta, \delta, \gamma, \sigma) = \int_\Omega W_c(\sigma)\, d\Omega - \int_{\Gamma_u} ((\sigma \cdot n) \cdot \bar{u})\, d\Gamma \tag{21b}$$

The constraint sets for the two operators in the inf-inf problem given in equation (21a) are given entirely in terms of the variable over which each individual infimum is sought, so the operators can be interchanged without changing the results. That is, we can first find the infimum of the complementary strain energy with respect to the densities (δ, γ) and the orientation of the direction of orthotropy with respect to the global axes (θ) and then find the infimum over the admissable stress fields. Introduction of, for example, displacement constraints at the outer design level of problem (21a) would destroy this feature. In the case of the sup-inf problem given by equation (20a), it is not obvious that the sup and inf operators can be interchanged. However, it has recently been demonstrated that finding the supremum of L_u with respect to θ and the ratio of δ to γ under fixed ρ can be carried out before taking the infimum of L_u over the kinematically admissible displacement fields without changing the results [30]. In the following, we interchange the sup and inf operators to arrive at subproblems that can be solved analytically. Diagrams of the optimization problems that are obtained by successive interchanges of the sup and inf operators in problem DP0 and the inf operators in problem SP0, each followed by analytical optimization of one of the microstructure design variables, are shown in Fig. 3. Each analytical solution of a subproblem leads to a reduced optimization problem with fewer unknowns. As explained in section 4.3.1, it is not possible to interchange the order of maximization over ρ and minimization over $\boldsymbol{u}$ in the second reduced problem DP2. Therefore, we cannot obtain a third reduced optimization problem in terms of the displacements only. The detailed

development of the reduced optimization problems, for both the displacement and stress formulations, is presented in the following sections.

4.1 FIRST REDUCED PROBLEM: ANALYTICAL OPTIMIZATION OF THE DIRECTION OF ORTHOTROPY (θ)

Equation (20a) in problem DP0 is equivalent to [30],

$$\underset{\delta,\gamma}{sup} \quad \underset{u}{inf} \quad \underset{\theta}{sup} \quad L_u(\theta, \delta, \gamma, u) \tag{22}$$

Similarly, equation (21a) in problem SP0 is equivalent to,

$$\underset{\delta,\gamma}{inf} \quad \underset{\sigma}{inf} \quad \underset{\theta}{inf} \quad L_\sigma(\theta, \delta, \gamma, \sigma) \tag{23}$$

The angle of orthotropy, θ, is the angle of rotation of the material axes relative to the global reference frame, while the principal angle, ψ, is the angle of rotation of the principal strain axes. Pedersen ([31], [32]) has shown that for a general orthotropic material the stiffest structure is obtained by aligning the material axes with the principal strain axes (for maximizing the potential energy) or the principal stress axes (for minimizing the complementary potential energy). That is, if we assume that $C_{1111} > C_{2222}$ and choose ε_I and ε_{II} such that $|\varepsilon_I| > |\varepsilon_{II}|$ the stiffest structure is obtained for $\theta = \psi$. This result is valid for any orthotropic material having low shear stiffness, that is materials which satisfy $C_{1111} + C_{2222} - 2C_{1122} - 4C_{1212} > 0$, which is the case for our rank-2 composite. Also, it is easy to see that the axes of principal stress, the axes of principal strain and the axes of orthotropy are aligned in the stiffest microstructure. Alternatively, one could appeal to the general bounding theorems of effective materials theory to reach the same conclusion, c.f. [20]. Next, we use this result to eliminate θ as a design variable.

4.1.1 *Displacement Formulation*

Noting the alignment of the principal axes and the optimal axes of orthotropy and by combining equations (3) and (8), we find that the strain energy density of any orthotropic material with an optimal material angle θ is given by,

$$W'(\varepsilon) = \frac{1}{2}(C_{1111}\varepsilon_I^2 + C_{2222}\varepsilon_{II}^2 + 2C_{1122}\varepsilon_I\varepsilon_{II}) \tag{24}$$

The principal strains, ε_I and ε_{II}, can be expressed in terms of the Cartesian strain components to get the following expressions for the strain energy density.

$$(\varepsilon_{xx}+\varepsilon_{yy}) \geq 0 \;:\; W'(\varepsilon) = \frac{(2\alpha_1(\varepsilon_{xx}^2+\varepsilon_{yy}^2) + 8C_{1122}\varepsilon_{xx}\varepsilon_{yy} + \beta_1\gamma_{xy}^2 + 2\alpha_2\kappa(\varepsilon_{xx}+\varepsilon_{yy}))}{8}$$

$$(\varepsilon_{xx}+\varepsilon_{yy}) \leq 0 \;:\; W'(\varepsilon) = \frac{(2\alpha_1(\varepsilon_{xx}^2+\varepsilon_{yy}^2) + 8C_{1122}\varepsilon_{xx}\varepsilon_{yy} + \beta_1\gamma_{xy}^2 - 2\alpha_2\kappa(\varepsilon_{xx}+\varepsilon_{yy}))}{8} \tag{25}$$

where $\alpha_1 = C_{1111} + C_{2222}$, $\alpha_2 = C_{1111} - C_{2222}$, $\beta_1 = C_{1111} + C_{2222} - 2C_{1122}$ and $\kappa = \sqrt{(\varepsilon_{xx}-\varepsilon_{yy})^2 + \gamma_{xy}^2}$.

The strain energy density function described by equation (25) is that of a fictitious "adaptive" rank-2 material whose material axes rotate so as to always remain coincident with the instantaneous principal strain axes. Even though our rank-2 composite is constructed from a linear elastic material, the response of the rotating adaptive material is nonlinear elastic, as can be seen in equation (25). An effective tangent material stiffness matrix for the adaptive material can be derived based on the energy density function in equation (25). The tangent stiffness matrices for the two cases, $\varepsilon_{xx}+\varepsilon_{yy} < 0$ and $\varepsilon_{xx}+\varepsilon_{yy} > 0$ are distinct and positive definite. However, the tangent stiffness matrix and the stresses are discontinuous for $\varepsilon_{xx}+\varepsilon_{yy} = 0$ ($\varepsilon_I = -\varepsilon_{II}$) and some of the terms in the tangent stiffness matrix are unbounded for $\kappa = 0$ ($\varepsilon_I = \varepsilon_{II}$). These problems are eliminated for a rank-2 layered material if the layer densities δ and γ are continuously optimized as in section 4.2.1.

After carrying out the maximization over θ in equation (22), we get the following displacement formulation.

- Displacement problem DP1:

$$\sup_{\delta,\gamma} \quad \inf_{u \in V_u} \quad L'_u(\delta, \gamma, \boldsymbol{u}) \tag{26a}$$

subject to $0 \le \delta \le 1$, $0 \le \gamma \le 1$, $\rho = \delta + \gamma - \gamma\delta$ and $\int_\Omega \rho d\Omega = \bar{V}$;

$$L'_u(\delta, \gamma, \boldsymbol{u}) = \int_\Omega W'(\varepsilon(u))\, d\Omega - \int_{\Gamma_t} (\bar{\boldsymbol{t}} \cdot \boldsymbol{u})\, d\Gamma - \int_\Omega (\boldsymbol{b} \cdot \boldsymbol{u})\, d\Omega \tag{26b}$$

4.1.2 Stress Formulation

If we enforce the optimal material angle $\theta = \psi$, then the complementary energy density is expressed in terms of the principal stresses σ_I and σ_{II} as,

$$W'_c(\sigma) = \frac{1}{2} \frac{(C_{1111}\sigma_{II}^2 + C_{2222}\sigma_I^2 - 2C_{1122}\sigma_I\sigma_{II})}{(C_{1111}C_{2222} - C_{1122}^2)} \tag{27}$$

After analytical optimization over the angle θ, the stress-based problem given by equation (23), is stated as,

- Stress problem SP1:

$$\inf_{\delta,\gamma} \quad \inf_{\sigma \in V_\sigma} \quad L'_\sigma(\delta, \gamma, \sigma) \tag{28a}$$

subject to $0 \le \delta \le 1$, $0 \le \gamma \le 1$, $\rho = \delta + \gamma - \gamma\delta$ and $\int_\Omega \rho d\Omega = \bar{V}$;

$$L'_\sigma(\delta, \gamma, \sigma) = \int_\Omega W'_c(\sigma)\, d\Omega - \int_{\Gamma_u} ((\sigma \cdot n) \cdot \bar{\boldsymbol{u}})\, d\Gamma \tag{28b}$$

4.2 SECOND REDUCED PROBLEM: ANALYTICAL OPTIMIZATION OF THE LAYER DENSITY δ

4.2.1 Displacement formulation

We can interchange the order of the maximization over δ and minimization over $\boldsymbol{u}$ in equation (26a) without changing the results [30]. Problem DP1 is restated as,

$$\sup_{\rho} \quad \inf_{\boldsymbol{u} \in V_u} \quad \sup_{\delta} \qquad L'_u(\delta, \rho, \boldsymbol{u}) \tag{29a}$$

subject to $0 \le \delta \le \rho \le 1$ and $\int_\Omega \rho d\Omega = \bar{V}$;

$$L'_u(\delta, \rho, \boldsymbol{u}) = \int_\Omega \tilde{W}'(\varepsilon(u))\, d\Omega - \int_{\Gamma_t} (\bar{\boldsymbol{t}} \cdot \boldsymbol{u})\, d\Gamma - \int_\Omega (\boldsymbol{b} \cdot \boldsymbol{u})\, d\Omega \tag{29b}$$

$\tilde{W}'(\varepsilon)$ is the same as $W'(\varepsilon)$ in equation (24), except that the elastic moduli are expressed as functions of δ and ρ (using equation (17)), rather than δ and γ.

For the displacement formulation, the Kuhn-Tucker optimality condition for the design variable δ is,

$$\frac{\partial}{\partial \delta} \tilde{W}'(\varepsilon) = 0 \tag{30}$$

if neither the upper nor the lower-bound constraints on δ are active. We have assumed that the layers of density δ are co-aligned with the ε_{II} strain direction in the optimal rank-2 composite (cf. Fig. 2) in arriving at the expression for $\tilde{W}'(\varepsilon)$. This does not guarantee that the material satisfies the condition $C_{1111} \ge C_{2222}$. However, it turns out that the optimization over δ automatically ensures that the resulting micro-structure satisfies this condition, in accordance with the results on optimal rotations of orthotropic materials.

Solving equation (30) gives two roots for the optimal layer density δ. We derived expressions for the two roots using lengthy hand-calculations and confirmed them using a symbolic computation package. The corresponding optimal layer densities γ can be de-

rived from equation (17) as a function of ρ and the principal strains. The expressions for the optimal layer densities according to equation (30) are given by equation (31). In the following, we use the term 'mode' to describe which expression for the optimal value of δ governs. For example, mode-I and mode-II materials are rank-2 composites where δ assumes the values of the alternative roots of equation (30). Mode-III represents a rank-2 composite in which the lower-bound constraint on δ is active.

$$\text{mode-I: } \delta = \frac{\varepsilon_I(1+\nu\rho-\rho)+\varepsilon_{II}}{\nu\varepsilon_I+(2-\rho-\nu+\nu\rho)\varepsilon_{II}} \qquad \text{mode-II: } \delta = \frac{\varepsilon_I(\nu\rho+\rho-1)+\varepsilon_{II}}{\nu\varepsilon_I+(2-\rho+\nu-\rho\nu)\varepsilon_{II}}$$

$$\gamma = \frac{\varepsilon_I+\varepsilon_{II}(1+\nu\rho-\rho)}{(1-\nu)(\varepsilon_I-\varepsilon_{II})} \qquad \gamma = \frac{\varepsilon_I+\varepsilon_{II}(\nu\rho+\rho-1)}{(1+\nu)(\varepsilon_I+\varepsilon_{II})}$$

$$\text{mode-III: } \delta = 0$$

$$\gamma = \rho \tag{31}$$

Note that the mode-III material (for the lower bound $\delta = 0$) represents a rank-1 layering in the 1-direction. Accordingly, the material can only sustain a uniaxial stress state in mode-III; this is consistent with the choice $|\varepsilon_I| \geq |\varepsilon_{II}|$. Also observe that the upper bound $\delta = \rho$ can only be achieved for the solid material $\rho = 1$. The effective properties of the mode-I, mode-II and mode-III materials all reduce to the properties of the solid isotropic material for $\rho = 1$. Moreover, the mode-I, mode-II and mode-III materials satisfy the constraint $\delta \leq \rho$ for $\rho \leq 1$, so the upper bound constraint on δ can be ignored. Substitution of the above expressions for the layer densities in equation (19) verifies that the resultant materials satisfy the condition $C_{1111} \geq C_{2222}$. In the special cases of $\varepsilon_I = -\varepsilon_{II}$ and $\varepsilon_I = \varepsilon_{II}$, it can be verified that $C_{1111} = C_{2222}$. Thus the problems which arise in the first reduced problem do not occur after optimization over layer densities.

The ranges of validity for mode-I, mode-II and mode-III materials as functions of ρ and the principal strain ratio $k = \varepsilon_{II}/\varepsilon_I$ are given next (see Fig. 4a). Since by convention

$|\varepsilon_I| \geq |\varepsilon_{II}|$, we have $-1 \leq k \leq 1$. The criterion that $0 < \delta \leq \rho$ in the mode-I and mode-II regions in equation (31) gives,

$$\text{mode-I: } \frac{1+k}{1-\nu} < \rho \leq 1 \qquad \text{mode-II: } \frac{1-k}{1+\nu} < \rho \leq 1 \tag{32}$$

Finally, for mode-III we have,

$$\text{mode-III: } 0 \leq \rho \leq min\left(\frac{1+k}{1-\nu}, \frac{1-k}{1+\nu}\right) \tag{33}$$

Combining the expressions for the optimal layer densities (equation (31)), the effective material properties (equation (19)) and the strain energy density (equation (24)), we get the following expressions for the strain energy density of the optimized rank-2 material.

$$\begin{aligned}
\text{mode-I: } W''(\rho, \varepsilon) &= \frac{E\left(\varepsilon_I^2 + 2\varepsilon_I\varepsilon_{II}(1-\rho+\nu\rho) + \varepsilon_{II}^2\right)}{2(1-\nu)(2-\rho+\nu\rho)} \\
\text{mode-II: } W''(\rho, \varepsilon) &= \frac{E\left(\varepsilon_I^2 - 2\varepsilon_I\varepsilon_{II}(1-\rho-\nu\rho) + \varepsilon_{II}^2\right)}{2(1+\nu)(2-\rho-\nu\rho)} \\
\text{mode-III: } W''(\rho, \varepsilon) &= \frac{1}{2}\rho E\varepsilon_I^2
\end{aligned} \tag{34}$$

The expressions in equation (34) can be written directly in terms of the Cartesian strain components as,

$$\begin{aligned}
\text{mode-I: } W''(\rho, \varepsilon) &= \frac{E\left(\varepsilon_{xx}^2 + \varepsilon_{yy}^2 + \gamma_{xy}^2/2 + 2(1-\rho+\nu\rho)\left(\varepsilon_{xx}\varepsilon_{yy} - \gamma_{xy}^2/4\right)\right)}{2(1-\nu)(2-\rho+\nu\rho)} \\
\text{mode-II: } W''(\rho, \varepsilon) &= \frac{E\left(\varepsilon_{xx}^2 + \varepsilon_{yy}^2 + \gamma_{xy}^2/2 - 2(1-\rho-\nu\rho)\left(\varepsilon_{xx}\varepsilon_{yy} - \gamma_{xy}^2/4\right)\right)}{2(1+\nu)(2-\rho-\nu\rho)}
\end{aligned} \tag{35}$$

$W''(\rho, \varepsilon)$ for a mode-III material is given by equation (25) with $\alpha_1 = \alpha_2 = \beta_1 = \rho E$ and $C_{1122} = 0$ (since $\delta = 0$).

Equation (35) corresponds to the strain energy density function of a fictitious hyperelastic material, composed of an adaptive rank-2 composite with fixed bulk density ρ, whose material axes rotate so as to remain aligned with the instantaneous principal strain

axes and in which the layer densities are continuously adjusted (according to equation (31)) to remain optimal under the current strain state. Surprisingly, the resulting stress-strain relations ($\sigma_{ij} = \frac{\partial W''}{\partial \varepsilon_{ij}}$), for both the mode-I and the mode-II materials, are linear.

$$\text{mode-I:}\quad \sigma_{xx} = \frac{E\,(\varepsilon_{xx} + (1-\rho+\nu\rho)\,\varepsilon_{yy})}{(1-\nu)\,(2-\rho+\nu\rho)} \qquad \text{mode-II:}\quad \sigma_{xx} = \frac{E\,(\varepsilon_{xx} - (1-\rho-\nu\rho)\,\varepsilon_{yy})}{(1+\nu)\,(2-\rho-\nu\rho)}$$

$$\sigma_{yy} = \frac{E\,(\varepsilon_{yy} + (1-\rho+\nu\rho)\,\varepsilon_{xx})}{(1-\nu)\,(2-\rho+\nu\rho)} \qquad \sigma_{yy} = \frac{E\,(\varepsilon_{yy} - (1-\rho-\nu\rho)\,\varepsilon_{xx})}{(1+\nu)\,(2-\rho-\nu\rho)}$$

$$\sigma_{xy} = \frac{E\rho\,(1-\nu)\,\gamma_{xy}}{2\,(1-\nu)\,(2-\rho+\nu\rho)} \qquad \sigma_{xy} = \frac{E\gamma_{xy}}{2\,(1+\nu)} \tag{36}$$

The layering of the rank-1 material corresponding to mode-III is colinear with the numerically larger (ε_I) principal strain direction. This also generates a constitutive model equivalent to that of an adaptive hyperelastic material. However, in this case the effective stress-strain relation is nonlinear and the tangent stiffness matrix is singular. Nonetheless, one can derive a positive-definite secant material stiffness matrix for the mode-III region which is continuous at the mode-I/mode-III and mode-II/mode-III boundaries (see Fig. 4a) and which generates stresses that are consistent with the rank-1 microstructure (see section 7).

Equation (36) is rearranged to obtain the mode-I and mode-II material stiffness matrices.

mode-I material:

$$C = C''(\rho, E, \nu) = \tilde{E}\begin{bmatrix} 1 & 1-\rho+\nu\rho & 0 \\ 1-\rho+\nu\rho & 1 & 0 \\ 0 & 0 & \frac{(1-\nu)\rho}{2} \end{bmatrix} \tag{37}$$

$$\tilde{E} = \frac{E}{(1-\nu)\,(2-\rho+\nu\rho)}$$

mode-II material:

$$\boldsymbol{C} = C''(\rho, E, \nu) = \tilde{E}\begin{bmatrix} 1 & -(1-\rho-\nu\rho) & 0 \\ -(1-\rho-\nu\rho) & 1 & 0 \\ 0 & 0 & \dfrac{(2-\rho-\nu\rho)}{2} \end{bmatrix} \tag{38}$$

$$\tilde{E} = \frac{E}{(1+\nu)\,(2-\rho-\nu\rho)}$$

For $\rho = 1$, both the mode-I and the mode-II material stiffness matrices coincide with the stiffness matrix of a solid isotropic material without microstructure. That is,

$$\boldsymbol{C}''(1, E, \nu) = \boldsymbol{C}_{solid}(E, \nu) \tag{39}$$

In the development above, we chose to align the layer of density δ with the ε_{II} strain direction. If we alternatively choose to align this layer with the ε_I strain direction, then the optimization over δ results in the same energy expressions as above. That is, for each strain field there exist two optimal rank-2 microstructures, each having the same effective properties. In essence, aligning with the ε_I direction corresponds to extending the above analysis to the case $|\varepsilon_I| \le |\varepsilon_{II}|$. The optimal densities in this case are still given by equations (31), with the exception that mode-III is now a uniaxial structure in the δ direction, corresponding to $\delta = \rho$ and $\gamma = 0$. The conditions (32) and (33), expressing the ranges of the various modes, also extend readily to the alternative case, but with $1/k$ substituted for k.

After carrying out the optimization over the layer density δ in equation (29a), the second reduced form of the displacement problem is obtained.

- Displacement problem DP2:

$$\sup_{\rho} \quad \inf_{\boldsymbol{u} \in V_u} \quad L_u''(\rho, \boldsymbol{u}) \tag{40a}$$

subject to $0 \le \rho \le 1$ and $\int_\Omega \rho\, d\Omega = \bar{V}$; where

$$L''_u(\rho, u) = \int_\Omega W''(\rho, \varepsilon(u))\, d\Omega - \int_{\Gamma_t} (\bar{t} \cdot u)\, d\Gamma - \int_\Omega (b \cdot u)\, d\Omega \qquad (40b)$$

4.2.2 Stress formulation

We interchange the order of the minimization over δ and minimization over σ to carry out the analytical optimization over the layer density δ. Problem SP1 can be restated as,

$$\inf_{\rho} \quad \inf_{\sigma \in V_\sigma} \quad \inf_{\delta} \quad L'_\sigma(\delta, \rho, \sigma) \qquad (41a)$$

subject to $0 \le \delta \le \rho \le 1$ and $\int_\Omega \rho\, d\Omega = \bar{V}$; where

$$L'_\sigma(\delta, \rho, \sigma) = \int_\Omega \tilde{W}'_c(\sigma)\, d\Omega - \int_{\Gamma_u} ((\sigma \cdot n) \cdot \bar{u})\, d\Gamma \qquad (41b)$$

$\tilde{W}'_c(\sigma)$ is the same as $W'_c(\sigma)$ in equation (27), except that the elastic moduli are expressed as functions of δ and ρ rather than δ and γ.

If the upper and lower bound constraints on δ are not active, the optimality condition is,

$$\frac{\partial}{\partial \delta} \tilde{W}'_c(\sigma) = 0 \qquad (42)$$

The optimal layer densities for the mode-I and mode-II materials can be computed analytically as,

$$\delta = \frac{\rho|\sigma_{II}|}{|\sigma_{II}| + (1-\rho)|\sigma_I|} \qquad \gamma = \frac{\rho|\sigma_I|}{|\sigma_I| + |\sigma_{II}|} \qquad (43)$$

The absolute value terms appearing in equations (43) indicate different expressions for the optimal layer densities δ and γ for the mode-I and mode-II cases. In particular, $\sigma_I\sigma_{II} < 0$ indicates a mode-I material and $\sigma_I\sigma_{II} > 0$ indicates a mode-II material (see Fig. 4b). Similar to the displacement formulation, the mode-III material corresponds to a uniaxial stress state ($\sigma_{II} = 0$) so that $\delta = 0$ and $\gamma = \rho$.

Substituting the expressions for the optimal layer densities in equation (27), we get the expressions for the complementary strain energy of an optimized rank-2 material with fixed density ρ.

$$\begin{aligned}
\text{mode-I: } W_c''(\rho, \sigma) &= \frac{\sigma_I^2 - 2\sigma_I\sigma_{II}(1-\rho+\nu\rho) + \sigma_{II}^2}{2E\rho} \\
\text{mode-II: } W_c''(\rho, \sigma) &= \frac{\sigma_I^2 + 2\sigma_I\sigma_{II}(1-\rho-\nu\rho) + \sigma_{II}^2}{2E\rho} \\
\text{mode-III: } W_c''(\rho, \sigma) &= \frac{\sigma_I^2}{2E\rho}
\end{aligned} \tag{44}$$

Expressing the principal stresses in terms of the Cartesian stress components, we obtain the material compliance matrix $\boldsymbol{D}$, where $W_c'' = \frac{1}{2}\sigma^T\boldsymbol{D}\sigma$.

$$\begin{aligned}
\text{mode-I: } \boldsymbol{D} = \boldsymbol{D}''(\rho, E, \nu) &= \frac{1}{E\rho}\begin{bmatrix} 1 & -(1-\rho+\nu\rho) & 0 \\ -(1-\rho+\nu\rho) & 1 & 0 \\ 0 & 0 & 2(2-\rho+\nu\rho) \end{bmatrix} \\
\text{mode-II: } \boldsymbol{D} = \boldsymbol{D}''(\rho, E, \nu) &= \frac{1}{E\rho}\begin{bmatrix} 1 & 1-\rho-\nu\rho & 0 \\ 1-\rho-\nu\rho & 1 & 0 \\ 0 & 0 & 2\rho(1+\nu) \end{bmatrix}
\end{aligned} \tag{45}$$

The tangent material compliance matrix for a mode-III material can be derived by a method similar to the one used to derive the tangent stiffness matrix in the displacement formulation. In equation (45), we again see that the effective material behavior is linearly elastic and that $\boldsymbol{D}''^{-1} = \boldsymbol{C}''$ for both the mode-I and mode-II materials.

We now show the correspondence between the stress-based and displacement-based formulations. We first derive the principal stress-principal strain relationship for the mode-I and mode-II materials using equation (44). Inverting that relationship we obtain expressions for the principal stresses in terms of the principal strains.

$$\begin{aligned}
\text{mode-I: } (\sigma_I \sigma_{II} < 0) \ : \ \sigma_I &= \frac{E\,(\varepsilon_I + (1-\rho+\nu\rho)\,\varepsilon_{II})}{(1-\nu)\,(2-\rho+\nu\rho)} \\
\sigma_{II} &= \frac{E\,(\varepsilon_I (1-\rho+\nu\rho) + \varepsilon_{II})}{(1-\nu)\,(2-\rho+\nu\rho)} \\
\text{mode-II: } (\sigma_I \sigma_{II} > 0) \ : \ \sigma_I &= \frac{E\,(\varepsilon_I - (1-\rho-\nu\rho)\,\varepsilon_{II})}{(1+\nu)\,(2-\rho-\nu\rho)} \\
\sigma_{II} &= \frac{E\,(-\varepsilon_I (1-\rho-\nu\rho) + \varepsilon_{II})}{(1+\nu)\,(2-\rho-\nu\rho)}
\end{aligned} \tag{46}$$

The conditions $\sigma_I \sigma_{II} < 0$ and $\sigma_I \sigma_{II} > 0$ imposed on the principal stress expressions appearing in equation (46) give the same limits on ρ that appear in equation (32). The correspondence between the "$k - \rho$" diagram and the complementary "k_c-ρ" diagram is shown in Fig. 4.

After carrying out the analytical optimization over the layer density δ in equation (29a) the stress formulation can be stated as,

- Stress problem SP2:

$$\inf_{\rho} \quad \inf_{\sigma \in V_\sigma} \quad L''_\sigma(\rho, \sigma) \tag{47a}$$

subject to $0 \le \rho \le 1$ and $\int_\Omega \rho\, d\Omega = \bar{V}$; where

$$L''_\sigma(\rho, \sigma) = \int_\Omega W''_c(\rho, \sigma)\, d\Omega - \int_{\Gamma_u} ((\sigma \cdot n) \cdot \bar{u})\, d\Gamma \tag{47b}$$

4.3 THIRD REDUCED PROBLEM: ANALYTICAL OPTIMIZATION OF THE BULK DENSITY ρ

4.3.1 Displacement formulation

Analytical optimization of the layer directions and layer densities results in the effective strain energy density function given by expressions (34) and (35). This function is convex in the density ρ, as is readily checked by examining its second derivative for the different modes. This excludes the possibility of interchanging the inf and sup operators on u and ρ in problem DP2 and is consistent with the observations of ref. [30]. Hence, we cannot find a third reduced displacement problem.

4.3.2 Stress formulation

We interchange the order of the inf operators over σ and ρ in problem SP2 to obtain the equivalent problem,

$$\inf_{\sigma \in V_\sigma} \quad \inf_{\rho} \quad L_\sigma''(\rho, \sigma) \tag{48}$$

subject to $0 \le \rho \le 1$ and $\int_\Omega \rho d\Omega = \bar{V}$.

For the inner problem we obtain the stationary condition, $\frac{\partial}{\partial \rho} W_c''(\rho, \sigma) + \lambda = 0$, which is valid provided that the constraint $0 \le \rho \le 1$ is not active. λ is a scalar Lagrange multiplier for the volume constraint. By fairly straightforward algebraic manipulations, we get the following necessary condition for the optimal bulk density ρ:

$$\rho = \frac{|\sigma_I| + |\sigma_{II}|}{\sqrt{2\lambda E}} \text{ in all modes.} \tag{49}$$

The absolute value operators indicate that we have different expressions for the mode-I and mode-II materials. Examination of the second derivatives confirms that this stationary point is indeed a local minimum for the inner problem in ρ. Further, by inspection of the functional values for the stationary point and the limits on ρ, we see that the stationary point is in fact a global minimum.

Our result is equivalent to the one obtained by Allaire and Kohn ([13], [26]) by a direct relaxation method. They minimize the compliance functional J, while we minimize the complementary strain energy which is half the magnitude of J (equation (14)). Hence, the expression for the optimal density as given by equation (49) is the same as that obtained by Allaire and Kohn, except that the values of the Lagrange multipliers differ by a factor of 2.

The optimal distribution of the bulk density should satisfy the volume constraint:

$$\int_{\Omega} \rho d\Omega = \int_{\Omega} min\{\frac{|\sigma_I| + |\sigma_{II}|}{\sqrt{2\lambda E}}, 1\} d\Omega = \bar{V} \tag{50}$$

This constraint uniquely determines the value of the Lagrange multiplier λ for any meaningful volume constraint (that is, with a value less than the volume of the design domain Ω). The uniqueness follows from the monotonicity of ρ as a function of λ. Thus, the volume constraint in our case implies that we can consider λ as a unique function of the principal stresses, given by equation (50), and we can write $\lambda(\sigma_I, \sigma_{II})$. Therefore, we have arrived at a solution for the inner problem. The expressions for the complementary energy density corresponding to the optimal distribution of the bulk density are:

$$\text{if } \frac{|\sigma_I| + |\sigma_{II}|}{\sqrt{2E\lambda(\sigma_I, \sigma_{II})}} \le 1, \text{ then}$$

$$W_c'''(\sigma) = \frac{1}{2E}\{\sqrt{2E\lambda(\sigma_I, \sigma_{II})}\,(|\sigma_I| + |\sigma_{II}|) + 2(1-\nu)\sigma_I\sigma_{II}\} \text{ if } (\sigma_I\sigma_{II} \le 0)$$

$$W_c'''(\sigma) = \frac{1}{2E}\{\sqrt{2E(\lambda(\sigma_I, \sigma_{II}))}\,(|\sigma_I| + |\sigma_{II}|) - 2(1+\nu)\sigma_I\sigma_{II}\} \text{ if } (\sigma_I\sigma_{II} \ge 0) \quad (51)$$

$$\text{if } \frac{|\sigma_I| + |\sigma_{II}|}{\sqrt{2E\lambda(\sigma_I, \sigma_{II})}} \ge 1, \text{ then}$$

$$W_c'''(\sigma) = \frac{1}{2E}\{|\sigma_I|^2 + |\sigma_{II}|^2 + 2\nu|\sigma_I||\sigma_{II}|\}$$

The third reduced stress problem is obtained by combining equations (48) and (51).

- Stress problem SP3:

$$\inf_{\sigma \in V_\sigma} \quad L_\sigma'''(\sigma) \tag{52a}$$

where

$$L_\sigma''' = \int_\Omega W_c'''(\sigma)\, d\Omega - \int_{\Gamma_u} ((\sigma \cdot n) \cdot \bar{u})\, d\Gamma \tag{52b}$$

Although this problem involves only the single field variable σ, its solution is complicated by the fact that W_c''' is neither positive definite nor smooth.

5 Problem DP2 as a Mixed Variational Statement

The second reduced displacement problem DP2 is an inf-sup problem, corresponding to a two-field, mixed variational formulation. The stationary condition for problem DP2 with respect to $\boldsymbol{u}$ yields the usual weak form of the equilibrium equation, and the stationary condition with respect to the bulk density ρ yields a weak form of the optimality criterion,

$$\frac{\partial}{\partial \rho} W''(\rho, \boldsymbol{u}) - \lambda = 0 \tag{53}$$

which is valid provided that the constraint $0 \leq \rho \leq 1$ is not active. Here λ is a Lagrange multiplier for the volume constraint. These two equations (supplemented by the constraint equations) determine the two fields, $\boldsymbol{u}$ and ρ. As with any mixed variational problem, care must be taken in choosing the function spaces for $\boldsymbol{u}$ and ρ. Finite element formulations based on the problem DP2 must satisfy the Babuska-Brezzi stability conditions [35]. We discuss this matter in greater detail in sections 6 and 8.

6 Finite Element Model

We focus on the displacement formulation, which is compatible with the popular finite element stiffness method. A numerical implementation of the stress-based problem SP3 has been tested by Allaire and Kohn [26] and Allaire and Francfort [33]. Among the three displacement-based problems, DP2 involves the least number of design variables and guarantees an analytically optimal microstructure. We construct a mixed finite element method for DP2 in which the density and the displacement fields are parameterized as,

$$\begin{aligned} \boldsymbol{u} &= N_u \hat{\boldsymbol{u}} \\ \rho &= N_\rho \hat{\rho} \end{aligned} \tag{54}$$

N_u and N_ρ are matrices containing the displacement and density basis functions and $\hat{\boldsymbol{u}}$ and $\hat{\rho}$ are unknown parameter vectors. The choice of the basis functions for the displacement and density fields is critical to achieving a stable solution. When the domain is discretized using quadrilateral elements with an 8-node displacement model and a bilinear density field (possibly discontinuous across element boundaries), the solution is unstable in regions where the upper and lower bound constraints on the density are not active. Similarly, a discretization using a 4-node displacement model and a constant density distribution within each element and a discretization using a 9-node displacement model and a discontinuous bilinear density field generate unstable solutions. However, a mesh using an 8-node displacement model with a piecewise constant density distribution gives a stable solution. We attribute the problems of the unsuccessful models to Babuska-Brezzi type instabilities. Rodrigues reports stable solutions using a 9-node displacement model with a

piecewise constant density field [36]. Fig. 5 summarizes the stability properties of selected finite element models based on quadrilateral elements with discontinuous fields. Bendsøe, Diaz and Kikuchi [34] describe a stabilization scheme for a 4-node displacement model with a piece-wise constant density field that is based on a suitable weighting of the densities in a patch of four neighboring elements. This effectively introduces a type of 'super' element to the finite element formulation. This approach is similar to the Johnson and Pitkranta stabilization scheme for Stokes flow problems ([35], pg. 211).

It is tempting to construct an analogy between the present formulation of the topology design problem and the mixed finite element models for the Stokes problem. In particular, there is agreement between the dimensionality of the displacement and velocity fields and between the density and the pressure fields in the two problems. Indeed, the numerical results reported thus far show that the same elements work and fail for the two problems. However, the differential operators in the two problems are quite different, so theoretical results from the Stokes problem cannot be directly applied to the topology design problem where more work is needed to formulate the stability conditions.

7 Solution Method

We employ an iterative procedure to solve the mixed variational problem. We alternately solve the equilibrium problem for the displacement field, subject to a fixed distribution of bulk density, and optimize the bulk density distribution, subject to a fixed displacement field. An analytically optimal microstructure (for the current bulk density and displacement estimates) is maintained at all times. Although the stiffness analysis is nonlinear due to the rank-1 (mode-III) material, we carry out only one equilibrium iteration before updating the design. This serves to spread the cost of the nonlinear equilibrium iterations over a number of design cycles.

The redesign step is an iterative procedure.We seek a density distribution that satisfies equation (53) in a weak sense in the perforated region Ω_p where the bounds on ρ are inac-

tive. A pointwise optimality criterion scheme for the density field could be written as (cf. [5]),

$$\hat{\rho}^{k+1} = \left(\frac{1}{\lambda}\frac{\partial W''}{\partial \rho}\right)\rho^k \tag{55}$$

if the constraints $0 \le \rho \le 1$ are not violated. Since $\frac{\partial W''}{\partial \rho} \ge 0$, this update scheme can easily be extended to the full domain and to the finite element model as:

$$\begin{aligned} \hat{\rho}_\beta^{k+1} &= min\left\{\lambda^{-\eta} Z_\beta^k,\ 1.0\right\};\ \beta = 1, m \\ Z_\beta^k &= \left(\frac{\int_\Omega N_{\rho\beta}\left.\frac{\partial W''}{\partial \rho}\right|_{u^k} d\Omega}{\int_\Omega N_{\rho\beta} d\Omega}\right)^\eta \hat{\rho}_\beta^k\ ;\ \beta = 1, m \end{aligned} \tag{56}$$

where $N_{\rho\beta}$ is the β-th finite element basis function for the density field, $\hat{\rho}_\beta^k$ is the corresponding coefficient at iteration k, m is the dimension of $\hat{\rho}$ and u^k is the equilibrium displacement solution for the current density estimate. The exponent η can be adjusted to improve the stability and convergence properties of the update algorithm. Experience shows that good results are obtained for $\eta = 0.8$. In arriving at this update formula, we assume that each $N_{\rho\beta}$ does not change sign in Ω_p. This whole approach is a variation of an algorithm introduced by Cheng and Olhoff [12].

The update formula, equation (56), must be applied subject to the volume constraint. Note that equations (54) and (56) provide an explicit formula for the updated density field ρ^{k+1} as a function of the updated Lagrange multiplier. Thus, the volume of the updated design can be expressed as,

$$V(\lambda) = \int_\Omega \rho^{k+1}(\lambda)\, d\Omega \tag{57}$$

It can be shown that $V(\lambda)$ is a continuous function that is monotone decreasing with respect to λ in the range $V < \int_{\Omega} 1 d\Omega$. Furthermore, it is differentiable everywhere, except at (at most) a finite set of values of λ, with monotonically decreasing derivative. Specifically, $V(\lambda)$ is differentiable wherever $Z_\beta^k \neq \lambda^\eta$ for $\beta = 1, m$. These properties support the use of a Newton-Raphson iteration scheme to determine the unique value of λ that satisfies the volume constraint, $V(\lambda) = \bar{V}$. The iterations make use of the following expressions for the derivative of the volume with respect to the Lagrange multiplier at the points of differentiability.

$$\frac{\partial V}{\partial \lambda} = \sum_{\beta=1}^{m} \frac{\partial \hat{\rho}_\beta^{k+1}}{\partial \lambda} \int_{\Omega} N_{\rho\beta} d\Omega$$

$$\frac{\partial \hat{\rho}_\beta^{k+1}}{\partial \lambda} = \begin{cases} -\eta \lambda^{-(\eta+1)} Z_\beta^k & \text{if } (Z_\beta^k < \lambda^\eta) \\ 0 & \text{if } (Z_\beta^k > \lambda^\eta) \end{cases} \tag{58}$$

The density field is updated directly, via equations (54) and (56), after the new value of the Lagrange multiplier is obtained. This design is then used to initiate a stiffness analysis to update the displacement field to satisfy the equilibrium constraint.

The tangent stiffness matrix for a rank-1 (mode-III) material is singular and unsuitable for use in computation. Therefore, we have adopted an iterative solution strategy based on a secant stiffness matrix for the nonlinear equilibrium problem, rather than a conventional Newton-Raphson procedure based on the tangent stiffness matrix. The secant stiffness maps the total strain into the total stress, in contrast to a map from a strain increment to a stress increment as for the tangent stiffness. In the rank-2 regions (mode-I and mode-II) the response is linear, so the secant stiffness coincides with the linear stiffness matrices given in equations (37) and (38). We next derive a secant stiffness for the mode-III region that is positive definite, that is continuous with the mode-I and mode-II stiffnesses at the boundaries between the regions and that generates the correct stress distribution ($\sigma_I = \rho E \varepsilon_I$, $\sigma_{II} = 0$) everywhere in the mode-III material according to equation (3).

The conditions on the boundary of the mode-III region are given by equation (33). We substitute $\rho = \frac{1+k}{1-\nu}$ to eliminate ν in equation (37) to obtain the form of the mode-I stiffness at the boundary with the mode-III region. Similarly, we substitute $\rho = \frac{1-k}{1+\nu}$ into equation (38) to obtain the limiting form of the mode-II stiffness. We obtain the same result in either case:

$$C_{secant} = \frac{\rho E}{(1-k^2)} \begin{bmatrix} 1 & -k & 0 \\ -k & 1 & 0 \\ 0 & 0 & (\frac{1+k}{2}) \end{bmatrix} \tag{59}$$

It turns out that C_{secant} gives the desired uni-axial stress distribution for any values of the Cartesian strain components and for any value of the principal strain ratio k provided that k is compatible with the current strain state ($k = \varepsilon_{II}/\varepsilon_I$). Therefore equation (59) describes a secant stiffness relation for the entire mode-III region. Furthermore, the strain energy density described by the secant stiffness under this constraint is equal to the energy density W'' given in equation (34) for mode-III. The corresponding stress-strain relation is nonlinear because C_{secant} is a function of the current strain state. Accordingly, the secant stiffness must be updated at every equilibrium iteration, according to the local strain state at each point in the mode-III regions, until convergence is achieved.

8 Numerical Examples

Numerical examples are presented here to demonstrate the topology design formulation. Plane stress conditions are assumed, the thicknesses of the candidate regions are taken to be one in. and the material properties are $E = 2.1 \times 10^7$ psi and $\nu = 0.25$ in all the examples. The figures accompanying these examples display three aspects of the solutions: the bulk density distribution, the principal stress field and the microstructural design. Black regions in the bulk density plots represent a value of 1.0 (solid material), white regions represent a value of zero (voids) and gray regions represent areas with intermedi-

ate bulk density. A cross is drawn at the centre of each element in the principal stress plots, based on the centroidal values of principal stress. The lengths of the arms of the cross are proportional to the magnitudes of the principal stress components; the inclination of the cross indicates the principal stress orientation. Thus, a uniaxial principal stress is represented by a line segment aligned with the non-zero principal stress direction. The length of the segment is proportional to the principal stress magnitude. The microstructure design plots show layer densities and orientations computed by equation (31) based on centroidal strain values. These plots are drawn in essentially the same manner as the principal stress plots. The layers with density γ are aligned with the direction of the numerically larger principal strain.

Example 1:

This example illustrates that the aspect ratio of the candidate region can affect the topology of the design. We consider a cantilever beam loaded along its vertical edge (see Fig. 6a) with three different aspect ratios (l/h in Fig. 6a): $5/14$ (stubby cantilever), $8/5$ (medium cantilever) and $4/1$ (long cantilever). We use quadrilateral finite elements with 8-node displacement functions and constant density to model the structures. The specified volume fraction is 30% in all three cases.

i) Stubby cantilever: The dimensions are $l = 5$ in. and $h = 14$ in.. A 20×56 mesh of square elements is used to model the structure. We obtain the stable solution shown in Fig. 7, yielding $J = 176.65$ lb-in after 25 iterations. The aspect ratio of the candidate region allows struts to form at 45 degrees, so we get a design with two axial members and no shear infill. The plot of the principal stresses and angles (Fig. 8) reveals the axial stress state in the struts.

ii) Medium cantilever: The dimensions are $l = 8$ in. and $h = 5$ in.. A 40×25 mesh of square elements is used to model this example. We obtain the stable solution shown in Fig. 9 with $J = 3034$ lb-in after 25 iterations. In this case, the aspect ratio of the candidate region does not allow struts to form at 45 degrees between the load and the support. Instead, chords develop along the top and bottom edges which carry axial load; a shear web devel-

ops between the chords as seen in the principal stress plot (Fig. 10). Fig. 11 is a plot of the layer densities, δ and γ, in the final design. The top and bottom chords consist primarily of rank-1 material (except in regions near the support and the point load, where the bulk density is 1.0). The shear web is composed primarily of rank-2 composite material. The design is consistent with the finding that the chords carry uni-axial stresses while the shear web is subjected to a biaxial stress state.

iii) Long cantilever: In this example we have $l = 4$ in. and $h = 1$ in.. The mesh size is 32×8. The design obtained after 25 iterations has a compliance value of $J = 13895$ lb-in. and is shown in Fig 12. The chords carry uniaxial stress (Fig. 13), and a shear web develops between the chords similar to the medium cantilever example.

Example 2:

This example illustrates how an improper choice of the displacement and density interpolation functions can lead to numerical instabilities in the solution. A deep beam rests on two supports and is loaded along its top edge (see Fig. 6b). The specified volume fraction is 60%. "Checkerboard" instabilities were detected when half the structure is modeled using 320 4-node displacement/ constant density elements as shown in Fig. 14 (see discussion in Section 6 and [37]). When we use 8-node displacement/ constant density elements we obtain after 18 iterations the stable solution shown in Fig. 15, with $J = 72145$ lb-in.

Example 3:

This example illustrates that grey material (i.e., material with a bulk density between 0 and 1.0) is not limited to regions of biaxial response. The candidate region and loading conditions are shown in Fig. 6c. The specified volume fraction is 20%. A mesh of 32×40 8 node displacement/ constant density elements is used to model half the structure. The stable solution obtained after 25 iterations with $J = 159618$ lb-in, is shown in Fig. 16. The principal stress plot (Fig. 17) shows one region of grey material that carries radial uniaxial stress (similar to the spokes of a bicycle wheel), while the arch carries circumfer-

ential uniaxial stress (similar to the rim of a bicycle wheel). There is a solid region in the vicinity of the point load which is analogous to the hub of a wheel.

Our method works well for very low volume fractions. To illustrate this, we consider the same candidate region and loading conditions as above, but with a specified volume fraction of 10%. The structure does not 'break up' even at this low volume fraction (in contrast to the results obtained by other researchers), as seen in Fig. 18, and a stable well-behaved solution with $J = 299960$ lb-in is obtained after 25 iterations. The topology of the structure in this example is not affected by the change in the specified volume fraction (compare Figs. 16 and 18). Similar results were obtained for this example using a 5% volume fraction.

9 Conclusions

Analytical optimization of the microstructural parameters in the homogenized topology design problem leads to a series of reduced problems which form the basis for a family of computational solution procedures. The second reduced displacement problem DP2 appears to be an attractive choice for use with stiffness solution procedures. The interpretation of this formulation as a mixed variational problem has significant consequences with respect to the Babuska-Brezzi stability criterion in the construction of finite element models.

Although we have been able to get near-optimal designs with the current update strategy, terminal convergence is slow, and we would like to find a more effective redesign strategy. Another computational problem is associated with the non-uniqueness of the displacement solution for the rank-1 material in mode-III regions. This slows the convergence of the equilibrium iterations and introduces nonlinear character to what is otherwise a linear stiffness problem.

Currently, we carry out the optimization using a fixed finite element mesh. We plan to explore adaptive strategies to control error in both the displacement solution and the satisfaction of the optimality criterion for design. Thus, a unified method for adapting the mod-

els for $\boldsymbol{u}$ and ρ is needed. This will ensure accurate resolution of the optimal geometry and the corresponding displacement solution.

All of our current effort has been directed towards finding the exact solution to the relaxed form of the topology optimization problem. The relaxed problem can generate optimal designs in which parts of the structure have intermediate densities between zero and one. These solutions require some interpretation before they can be manufactured. One could alternatively attempt to manufacture the optimal microstructure or develop a macroscopic approximation of the microstructure (e.g. the spokes of a bicycle wheel are an effective substitute for the gray material in example 3). However, in many practical situations we would like our numerical procedure to directly generate a design that is comprised entirely of macroscopic solid and void regions. Hence, we plan to penalize intermediate densities to force all points to either a solid or void condition and to introduce various manufacturability constraints to address this problem. Extensions to three dimensions, multiple load cases, nonlinear materials and alternative objectives are also of interest.

ACKNOWLEDGEMENTS

The authors would like to thank the following organizations for their support of this work. The National Science Foundation (U.S.A.), the Danish Research Academy, the Danish Technical Research Council (Program for Research on Computer-Aided Design), Cray Research, Inc. and the Center for Supercomputing Research and Development. Computations were performed on the Cray Y-MP at the National Center for Supercomputing Applications.

References

[1] Y. Ding, 'Shape optimization of structures: a literature survey', Comp. Struct., 24, 985-1004 (1986)

[2] R. T. Haftka and R. V. Gandhi, 'Structural shape optimization- a survey', Comp. Meth. Appl. Mech. Engrg., 57, 91-106 (1986)

[3] R. B. Haber, D. A. Tortorelli, C. A. Vidal and D. G. Phelan, 'Design sensitivity analysis of nonlinear structures-I: Large deformation hyperelasticity and history-dependent material response', Structural Optimization: Status and Promise, M. P. Kamat (Ed.), AIAA Progress in Astronautics and Aeronautics series, 361-397 (1993)

[4] W. Prager and G. Rozvany, 'Optimization of structural geometry', Dynamical Systems, A. Bednarek and L. Cesari eds., Academic Press, 265-294 (1977)

[5] G. I. N. Rozvany, *Structural Design via Optimality Criteria*, Kluwer Academic Publishers, Dordrecht, The Netherlands, 1989

[6] J. Cea, A. Gioan and J. Michel, 'Quelques resultat sur l'idesntification de domaines', Calcolo III / IV (1973)

[7] R. V. Kohn and G. Strang, 'Optimal design and relaxation of variational problems', Comm. Pure Appl. Math., 39, 1-25 (Part-I), 139-182 (Part-II) and 353-377 (Part-III) (1986)

[8] F. Murat and L. Tartar, 'Calcul des variations et homogeneisation', Les Methodes de l'Homogeneisation: Theorie et Applications en Physique, Coll. de la Dir. des Etudes et Recherches de Electricite de France, Eyrolles, Paris, 319-370 (1985)

[9] L. Tartar, 'Estimation de coefficients homogeneises', Lecture Notes in Mathematics, Springer Verlag, Berlin, 704, 364-373 (1977)

[10] F. Murat, 'Conre-exemples pour divers problemes ou le controle intervient dans les coefficients' Ann. Mat. Pura ed Appl., Serie 4, 112, 49-68 (1977)

[11] A. K. Lurie, A.V. Fedorov, A.V. Cherkaev, 'Regularization of optimal design problems for bars and plates', J. Optim. Theory Appl., 37, 499-521 (Part-I) and 523-543 (Part-II) (1982)

[12] K. T. Cheng and N. Olhoff, 'An investigation concerning optimal design of solid elastic plates', Int. J. Solids Structures, 17, 305-323 (1981)

[13] R. Kohn, 'Composite materials and structural optimization', Proc. Workshop on Smart/Intelligent Materials and Systems, Honolulu, March, Technomic Press (1990)

[14] M. Bendsøe and N. Kikuchi, 'Generating optimal topologies in structural design using a homogenization method', Comp. Meth. Appl. Mech. Engrg., 71, 197-224 (1988)

[15] M. Avellaneda, 'Optimal bounds and microgeometries for elastic two-phase composites', SIAM J. App. Math., 47, 1216-1228 (1987)

[16] M. Avellaneda, 'Bounds on the effective elastic constants of two-phase composite materials', Proc. Sem. College de France, X, H. Brezis, J.-L. Lions (Eds), Pitman, London (1989)

[17] M. Avellaneda and G. W. Milton, 'Bounds on the effective elasticity tensor of composites based on two-point correlations', Proc. of the A.S.M.E Energy Technology Conference and Exposition, Houston, Texas (1989)

[18] K. Lurie and A. Cherkaev, 'The effective properties of composites and problems of optimal design of constructions', Uspekhi Mekhaniki, 9, 1-81 (1986) (in Russian)

[19] L. Gibianski and A. Cherkaev, 'Microstructures of composites of extremal rigidity and exact estimates of the associated energy density', Ioffe Physicotechnical Institute, preprint 1115, 1987

[20] G. Allaire and R.V. Kohn, 'Explicit optimal bounds on the elastic energy of a two-phase composite in two space dimensions', Courant Institute, New York University, New York, preprint (1991)

[21] G. Allaire and R. V. Kohn, 'Optimal bounds on the effective behavior of a mixture of two well-ordered elastic materials', Quar. Appl. Math., (to appear) (1992)

[22] A. Bensoussan, J. L. Lions and G. Papanicolaou, *Asymptotic Analysis for Periodic Structures*, North Holland, 1978

[23] Y. Grabovsky, 'Some microstructures minimizing the energy of a two phase composite in two space dimensions', Preprint, Courant Institute, NYU, New York, NY, USA (1992)

[24] G. Milton, 'On characterizing the set of possible effective tensors of composites: The variational method and the translation method', Comm. Pure Appl. Math., 43, 63-125 (1990)

[25] J. Goodman, R.V. Kohn and L. Reyna, 'Numerical study of a relaxed variational problem for optimal design', Comput. Meths. Appl. Mech. Engrg., 57, 107-127 (1986)

[26] G. Allaire and R. V. Kohn, 'Structural optimization using homogenization', Topology Optimization of Structures, M. P. Bendsøe and C. A. Mota Soares (Eds.), Kluwer Academic Publishers, Dordrecht, The Netherlands, 207-218 (to appear)

[27] I. S. Sokolnikoff, *Mathematical Theory of Elasticity*, Robert Krieger Publishing Company, Florida, 1987

[28] M. P. Bendsøe, 'Optimal shape design as a material distribution problem', Structural Optimization, 1, 193-202 (1989)

[29] G. A. Francfort and F. Murat, 'Homogenization and optimal bounds in linear elasticity', Arch. Rat. Mechs. Anal., 94, 307-334 (1986)

[30] R. Lipton, 'On implementation of partial relaxation for optimal structural compliance problems', Design with Advanced Materials, P. Pedersen (Ed.), Elsevier (to appear)

[31] P. Pedersen, 'On optimal orientation of orthotropic materials', Structural Optimization, 1, 101-106 (1989)

[32] P. Pedersen, 'Bounds on elastic energy in solids of orthotropic materials' Structural Optimization, 2, 55-63 (1990)

[33] G. Allaire and G. Francfort, 'A numerical structural optimization using homogenization', Topology Optimization of Structures, M. P. Bendsøe and C. A. Mota Soares (Eds.), Kluwer Academic Publishers, Dordrecht, The Netherlands, 239-249 (to appear)

[34] M. P. Bendsøe, A. Diaz and N. Kikuchi, 'Topology and generalized layout optimization of structures', Topology Optimization of Structures, M. P. Bendsøe and C. A. Mota Soares (Eds.), Kluwer Academic Publishers, Dordrecht, The Netherlands, 159-205 (to appear)

[35] F. Brezzi and M. Fortin, *Mixed and Hybrid Finite Element Methods*, Springer-Verlag, 1991

[36] H. C. Rodrigues and P. Fernandes, 'Topology optimization of linear elastic structures subjected to thermal loads', Topology Optimization of Structures, M.P. Bendsøe and C.A. Mota Soares (Eds.), Kluwer Academic Publishers, Dordrecht, The Netherlands, 437-450 (to appear)

[37] A. R. Diaz and N. Kikuchi, 'Solutions to shape and topology eigenvalue optimization problems using a homogenization method', Int. J. Numer. Meth. Eng., 35, 1487-1502 (1992)

List of figures

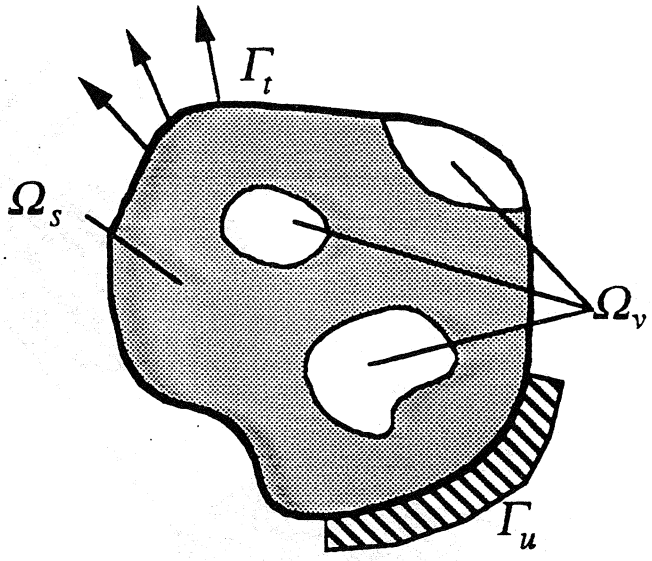

Figure 1 Domain diagram for the topology optimization problem.

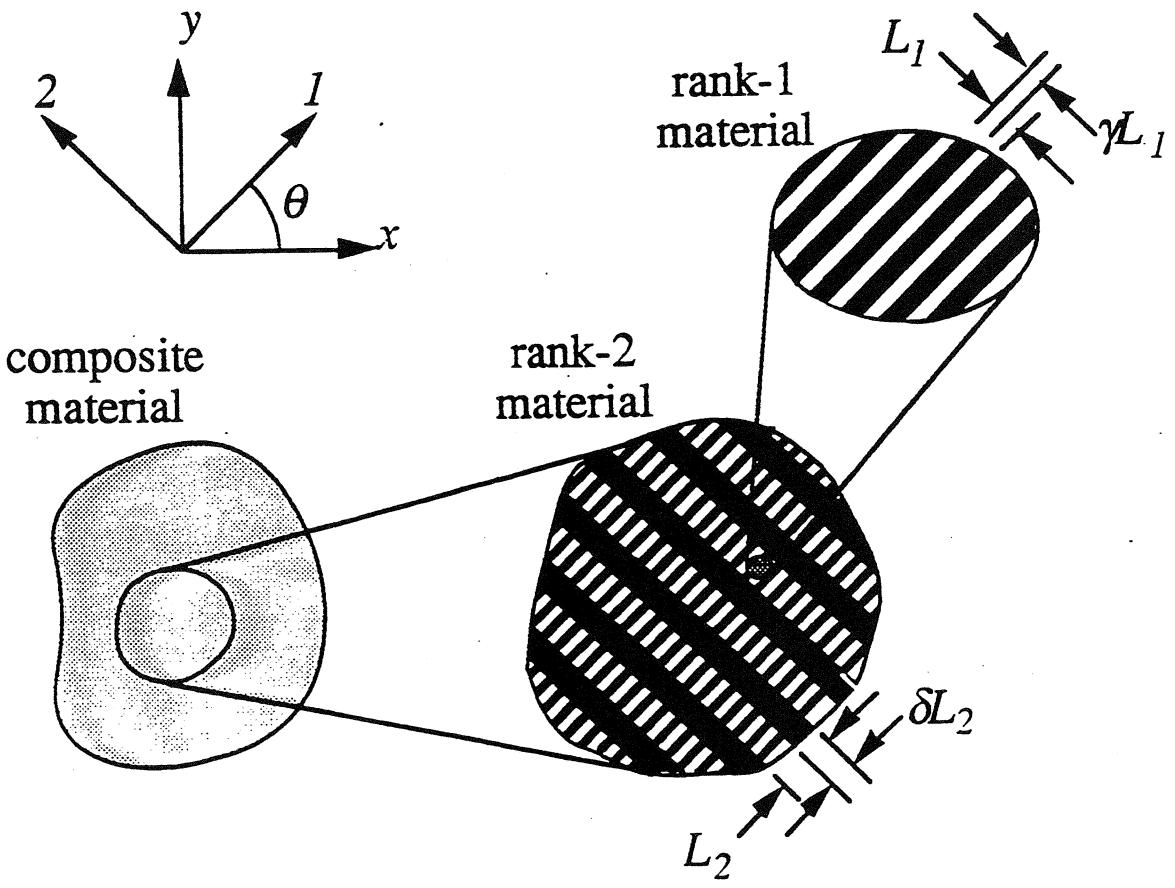

Figure 2. The structure of a rank-2, layered composite.

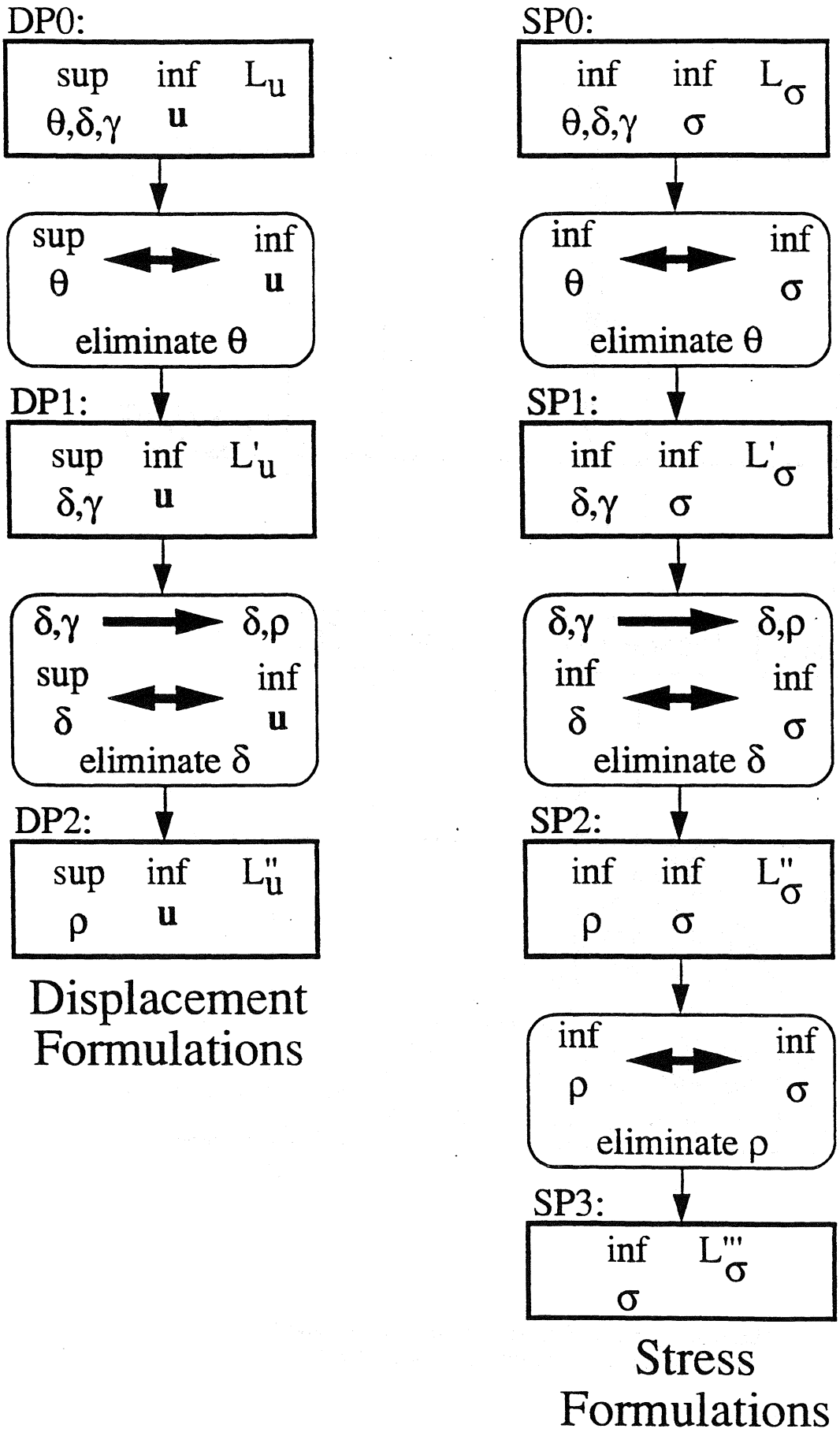

Figure 3. Procedures for generating reduced optimization problems.

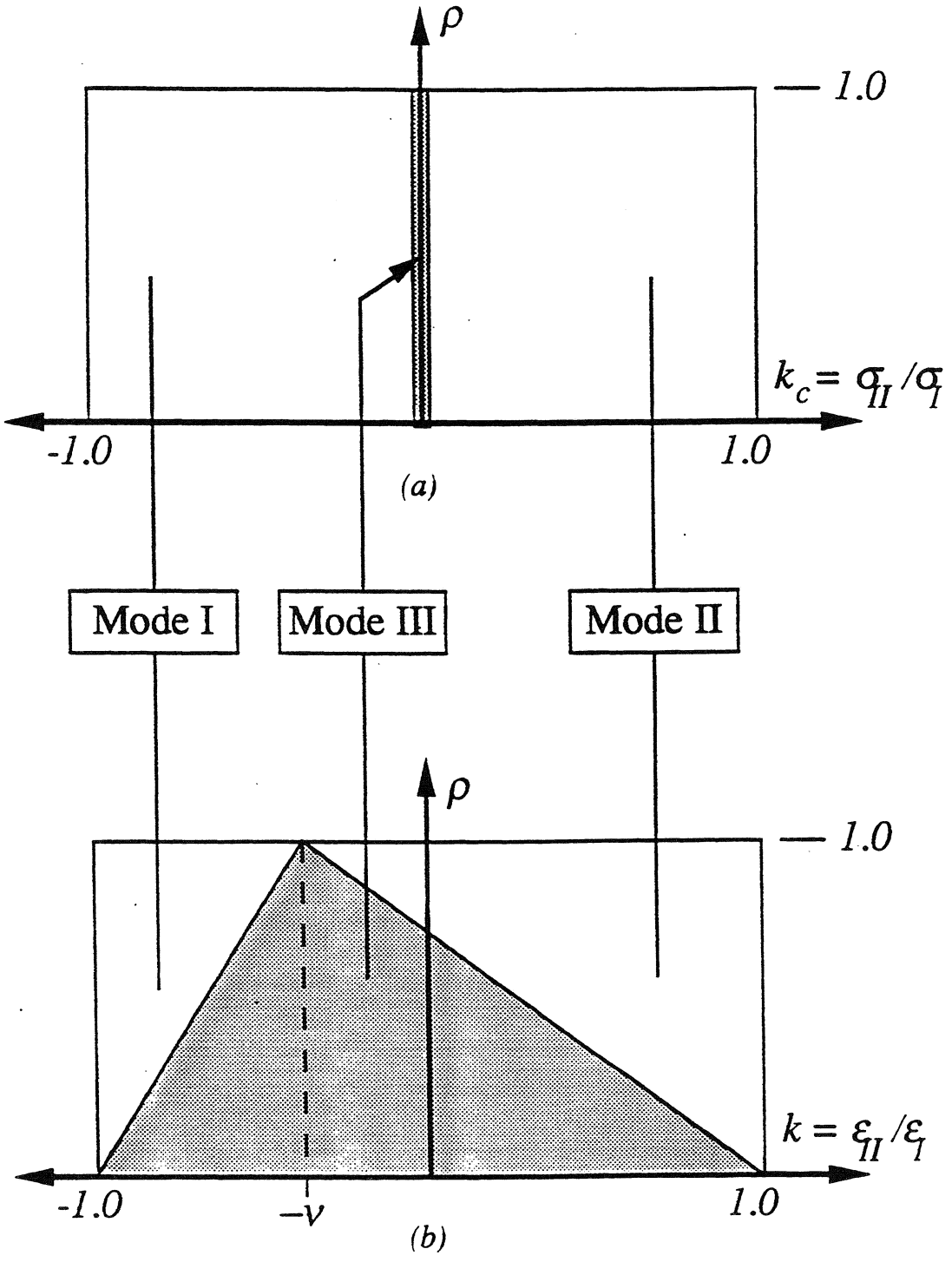

Figure 4. Ranges of validity for the various modes:
a) displacement method and b) stress method.

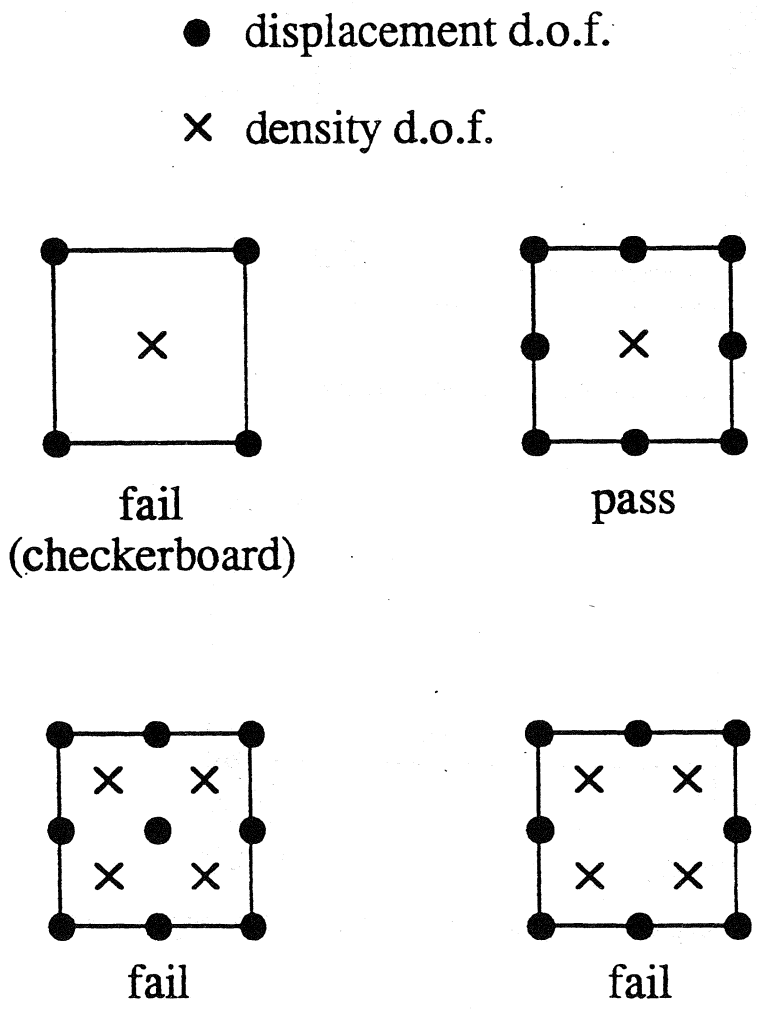

Figure 5. Stability of various mixed finite element models for the topology design problem with discontinuous density fields.

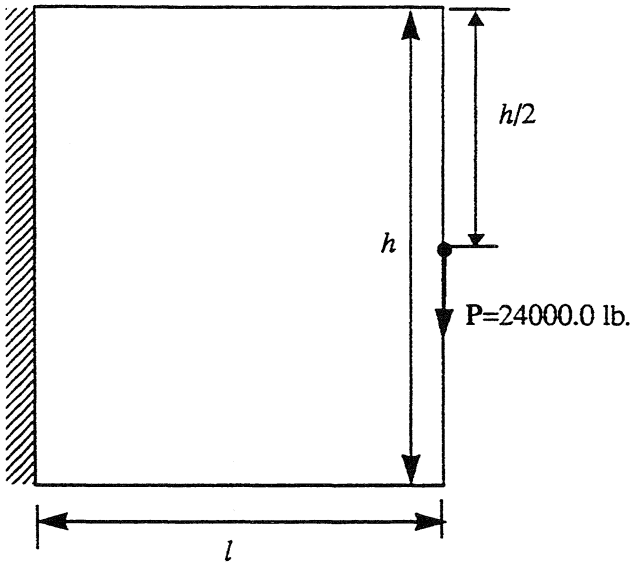

Fig. 6a Cantilever beam example

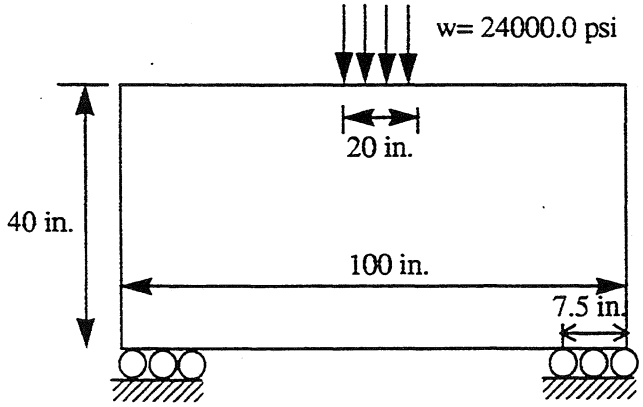

Fig.6b Deep beam with mid-span, distributed load on its top edge

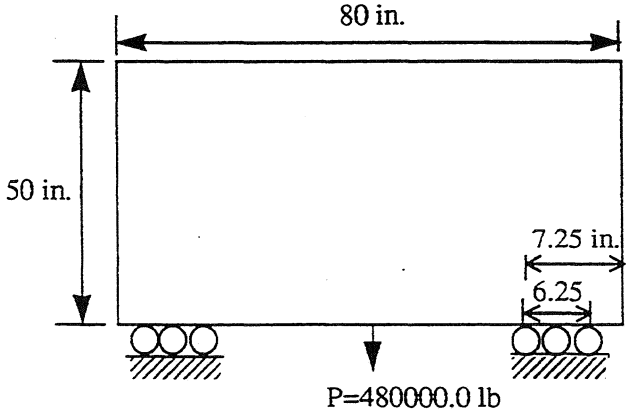

Fig. 6c Deep beam with mid-span, point load on its bottom edge

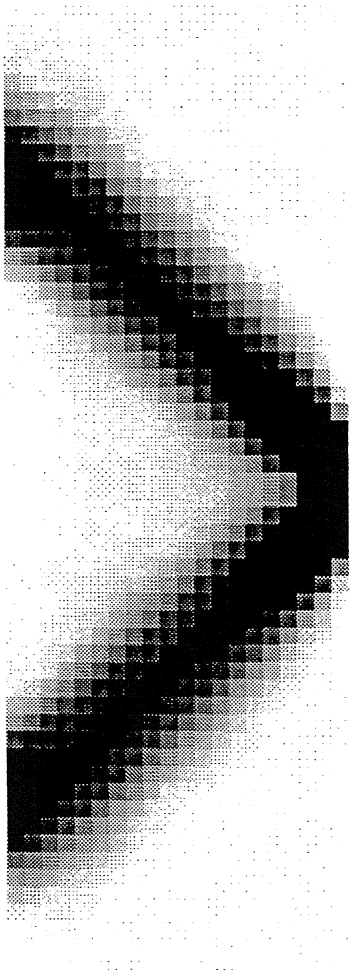

Fig. 7 Bulk density distribution for the stubby cantilever example

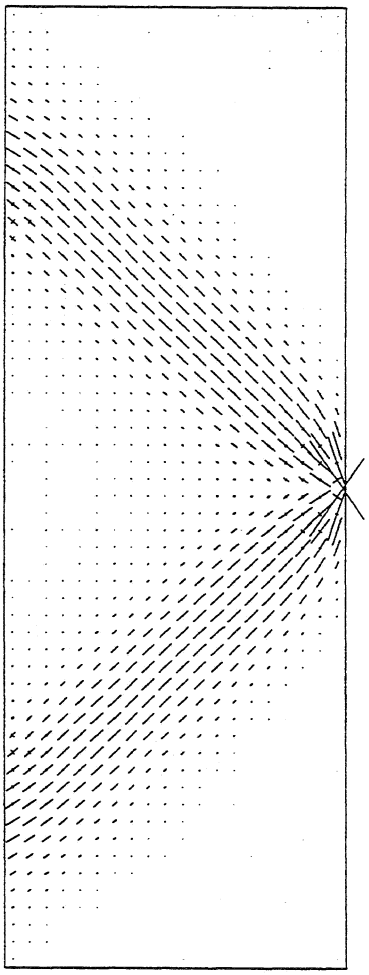

Fig. 8 Principal stress distribution for the stubby cantilever example

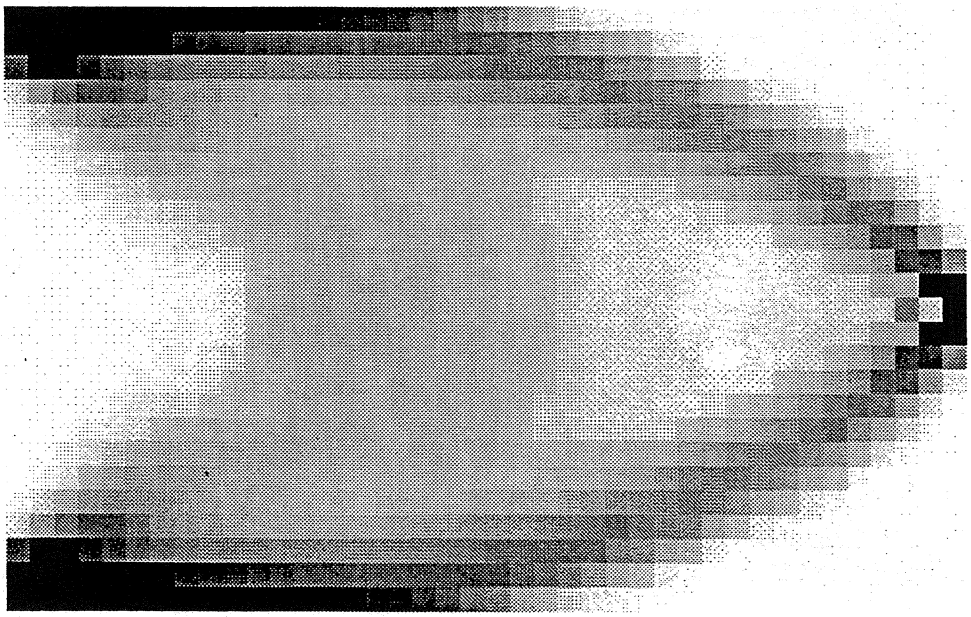

Fig. 9 Bulk density distribution for the medium aspect ratio cantilever example

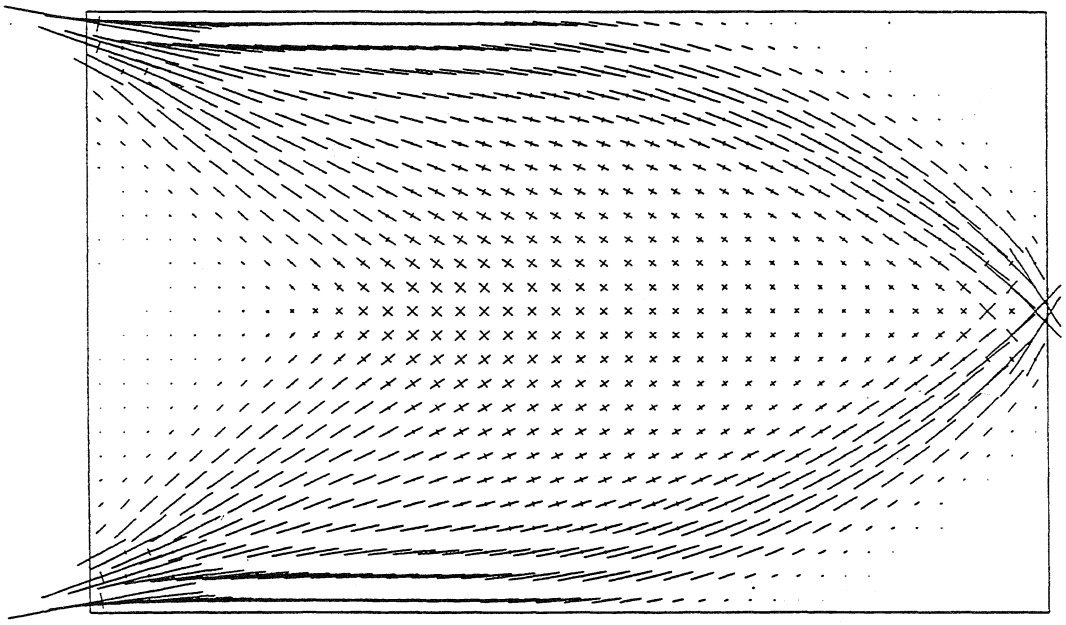

Fig. 10 Principal stress distribution for the medium aspect ratio cantilever example

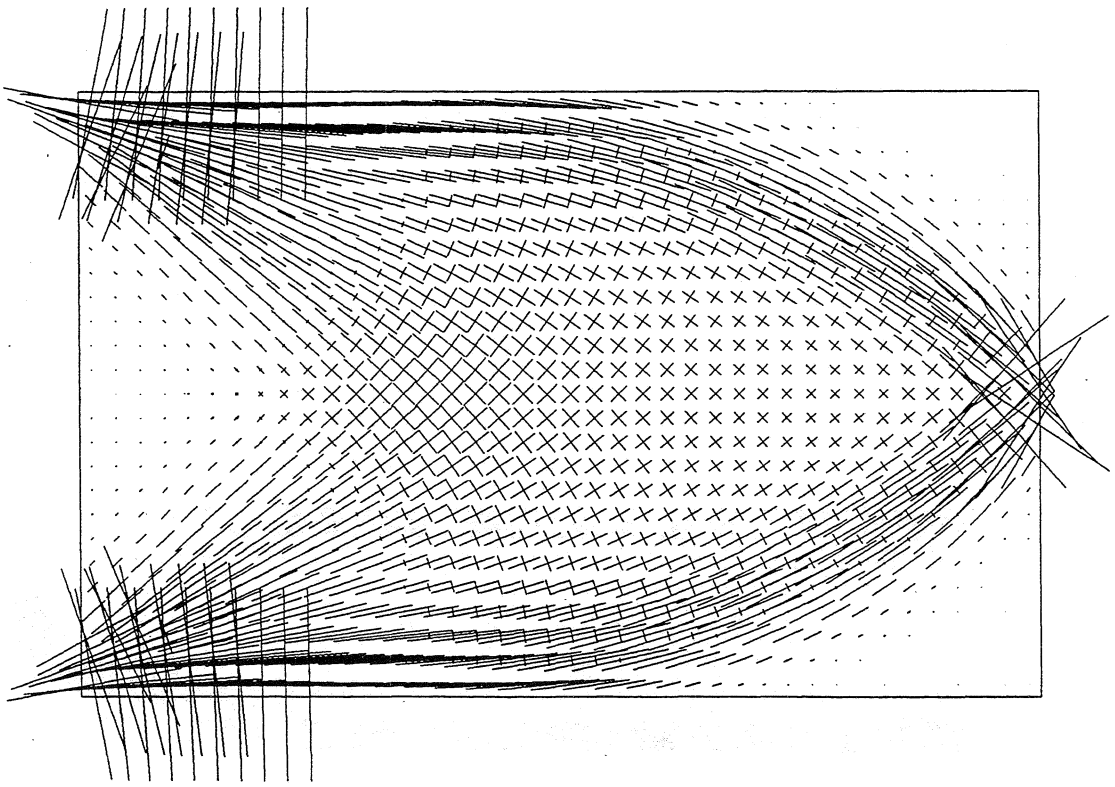

Fig. 11 Distribution of microstructure layer densities for the medium aspect ratio cantilever example

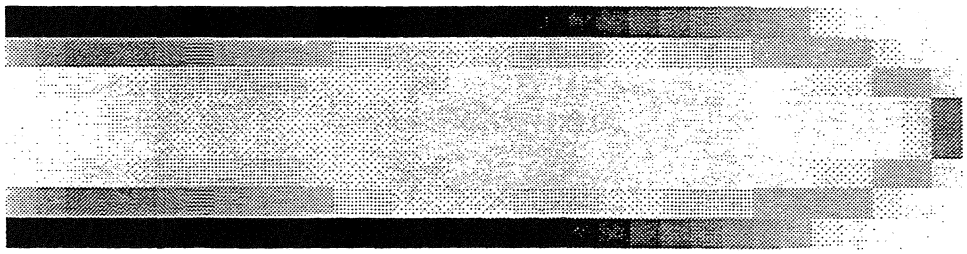

Fig. 12 Bulk density distribution for the long cantilever example

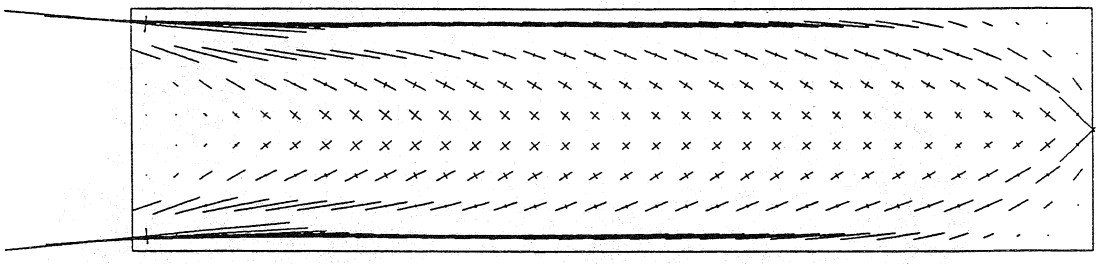

Fig. 13 Principal stress distribution for the long cantilever example

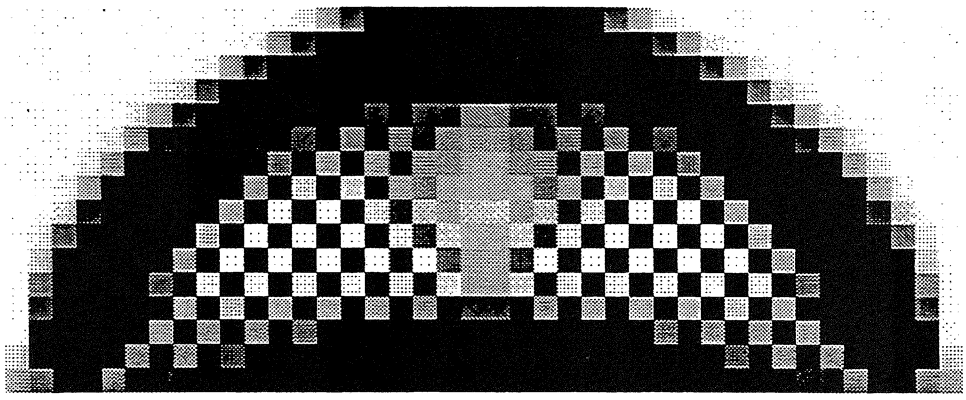

Fig. 14 Unstable 'checkerboard' solution obtained with 4-node displacement/ constant density elements

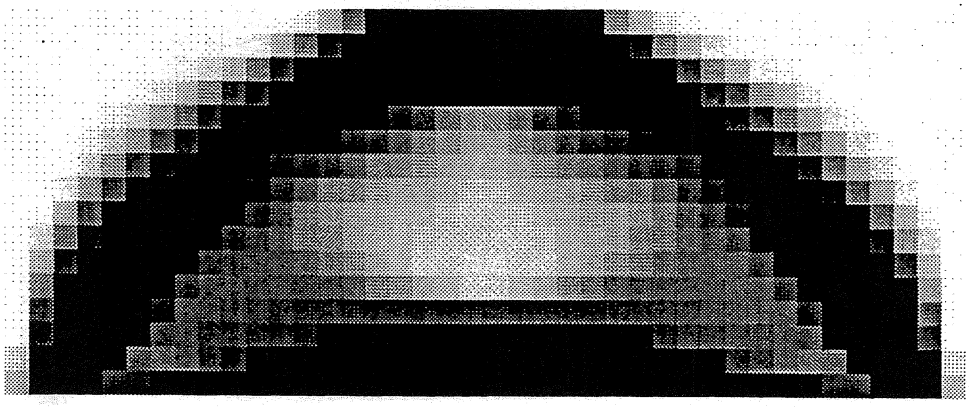

Fig. 15 Stable solution obtained with 8-node displacement/ constant density elements

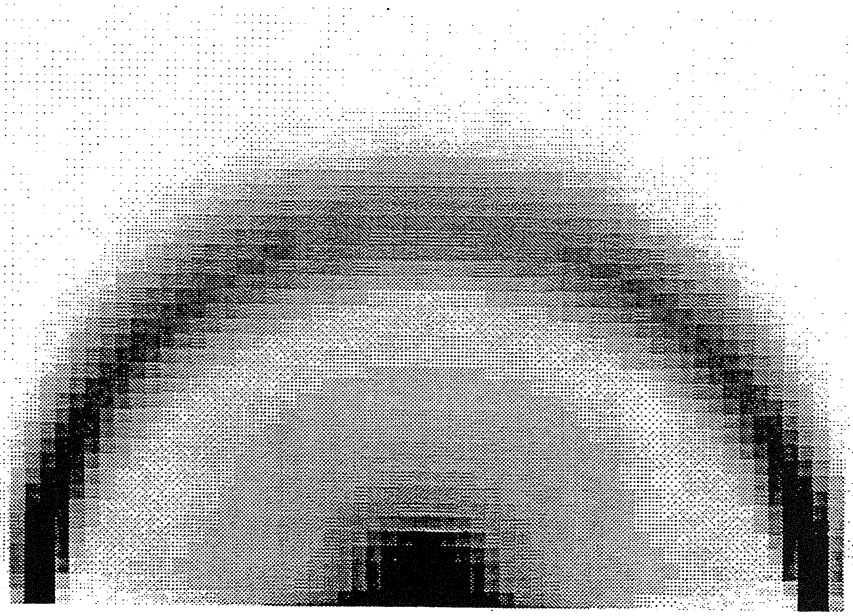

Fig. 16 Bulk density distribution for deep beam with mid-span load (bicycle wheel design)

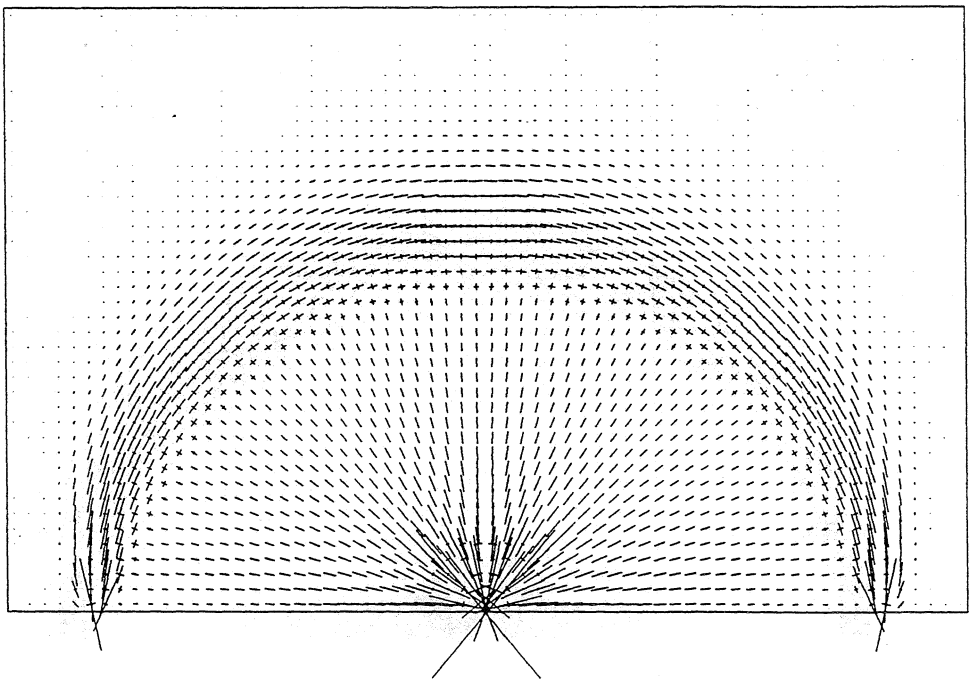

Fig. 17 Principal stress distribution for the bicycle wheel design

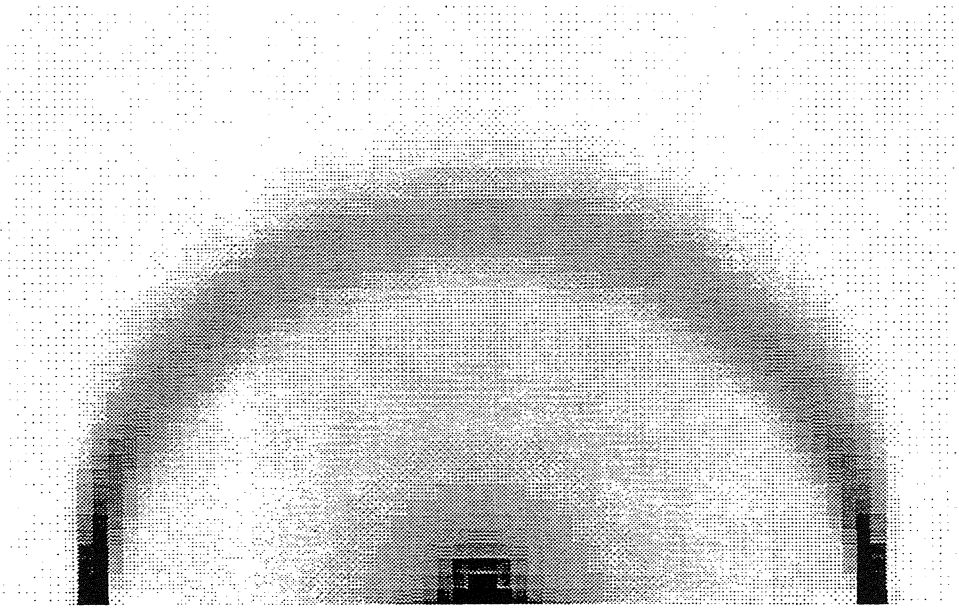

Fig. 18 Bulk density distribution for the bicycle wheel design with a 10% prescribed volume fraction

List of Recent TAM Reports

No.	*Authors*	*Title*	*Date*
483	Tung, A. T. C., R. J. Adrian, and B. G. Jones	Conditional velocity and Reynolds stresses in a plane turbulent shear layer	Feb. 1987
484	Jackson, T. L., A. K. Kapila, and D. S. Stewart	Evolution of a reaction center in an explosive material	Feb. 1987
485	Stewart, D. S., and J. B. Bdzil	A lecture on detonation-shock dynamics	Dec. 1987
486	Shawki, T. G.	Mathematical methods for engineers and physicists	Jan. 1988
487	Bohnert, M. J., G. B. Burwell, J. A. Ochs, S. A. Parks, T. J. Simeone, J. J. Sullivan, and B. R. Wagner	Twenty-fourth student symposium on engineering mechanics, M. E. Clark, coord. (1987)	Mar. 1988
488	Loewenherz, D. S., and C. J. Lawrence	Stability of viscous stratified free surface flows at low Reynolds number	Aug. 1988
489	Shawki, T. G.	Necessary and sufficient conditions for the onset of shear strain localization in thermal viscoplastic materials	Dec. 1988
490	Dasgupta, A.	An experimental investigation of homogeneous fatigue damage in a random short-fiber composite under combined tension-torsion loading	Dec. 1988
491	Lee, Hyung-In, and D. S. Stewart	Calculation of linear detonation instability—Part I: One-dimensional instability of plane detonation	Dec. 1988
492	Weaver, R. L.	Diffusivity of ultrasound in polycrystals	Feb. 1989
493	Shawki, T. G., R. J. Clifton, and Y. Kadioglu	Calculation of the viscoplastic response of polycrystals from slip theory for FCC single crystals	Mar. 1989
494	Toro, J. R.	Existence of weak solutions to the thick plate problem with various boundary conditions	Apr. 1989
495	Stewart, D. S., and B. W. Asay	Discrete modeling of beds of propellant exposed to strong stimulus	Apr. 1991
496	Klein, R., and D. S. Stewart	The relation between curvature, rate state dependence, and detonation velocity	Apr. 1991
497	Powers, J. M., and D. S. Stewart	Approximate solutions for oblique detonations in the hypersonic limit	Apr. 1991
498	Davidson, M. T., K. L. Kuster, K. W. Quinn, N. A. Sluz, and G. Stojkovich	Twenty-fifth student symposium on engineering mechanics, M. E. Clark, coord. (1988)	Feb. 1992
499	Cardenas, H. E., W. C. Crone, D. J. Scott, G. G. Stewart, and B. F. Tatting	Twenty-sixth student symposium on engineering mechanics, M. E. Clark, coord. (1989)	Mar. 1992
700	Juister, C. E., D. W. Newport, C. S. Payne, J. M. Peters, M. P. Thomas, and J. C. Trovillion	Twenty-seventh student symposium on engineering mechanics, M. E. Clark, coord. (1990)	Apr. 1992
701	Bernard, R. T., D. W. Claxon, J. A. Jones, V. R. Nitzsche, and M. T. Stadtherr	Twenty-eighth student symposium on engineering mechanics, M. E. Clark, coord. (1991)	Apr. 1992
702	Greening, L. E., P. J. Joyce, S. G. Martensen, M. D. Morley, J. M. Ockers, M. D. Taylor, and P. J. Walsh	Twenty-ninth student symposium on engineering mechanics, J. W. Phillips, coord. (1992)	May 1992
703	Kuah, H. T., and Riahi, D. N.	Instabilities and transition to chaos in plane wakes	Sept. 1992
704	Stewart, D. S., K. Prasad, and B. W. Asay	Simplified modeling of transition to detonation in porous energetic materials	Nov. 1992
705	Stewart, D. S., and J. B. Bdzil	Asymptotics and multi-scale simulation in a numerical combustion laboratory	Jan. 1993
706	Hsia, K. J., Y.-B. Xin, and L. Lin	Numerical simulation of semi-crystalline Nylon 6: Elastic constants of crystalline and amorphous parts	Jan. 1993
707	Hsia, K. J., and J. Q. Huang	Curvature effects on compressive failure strength of long fiber composite laminates	Jan. 1993
708	Jog, C.S., Haber, R.B., and M.P. Bendsoe	Topology design with optimized, self-adaptive materials	Mar. 1993